SIAM J. SCI. COMPUT.
Vol. 36, No. 5, pp. B835–B867

ENTROPY STABLE SPECTRAL COLLOCATION SCHEMES FOR THE NAVIER–STOKES EQUATIONS: DISCONTINUOUS INTERFACES*

MARK H. CARPENTER†, TRAVIS C. FISHER‡, ERIC J. NIELSEN†, AND STEVEN H. FRANKEL§

Abstract. Nonlinear entropy stability and a summation-by-parts framework are used to derive provably stable, polynomial-based spectral collocation element methods of arbitrary order for the compressible Navier–Stokes equations. The new methods are similar to strong form, nodal discontinuous Galerkin spectral elements but conserve entropy for the Euler equations and are entropy stable for the Navier–Stokes equations. Shock capturing follows immediately by combining them with a dissipative companion operator via a comparison approach. Smooth and discontinuous test cases are presented that demonstrate their efficacy.

Key words. high-order finite-element methods, conservation, skew-symmetric, entropy stability, Navier–Stokes, SBP-SAT

AMS subject classifications. 65N12, 65P40

DOI. 10.1137/130932193

1. Introduction.

Next generation numerical algorithms for use in large eddy simulations (LES) and hybrid Reynolds-averaged Navier–Stokes (RANS)-LES simulations will undoubtedly rely on efficient high-order formulations. Although high-order techniques are well suited for LES, most lack robustness when the solution contains discontinuities or even underresolved physical features. Although a variety of stabilization techniques have been developed for second-order methods (e.g., total variation diminishing (TVD) limiters [35], and entropy stability [40]), extending these techniques to high-order formulations has been problematic. High-order essentially nonoscillatory (ENO) [20, 36] and weighted ENO (WENO) [31, 25] schemes provide a partial remedy to the problem; they achieve high-order design accuracy away from captured discontinuities and maintain sharp "nearly monotone" captured shocks. Unfortunately, nonoscillatory schemes experience instabilities in less than ideal circumstances (e.g., curvilinear mapped grids or expansion of flows into vacuum). Because nonoscillatory schemes are largely based on stencil biasing heuristics rather than stability analysis, there is little theory to guide further development efforts focused on

*Submitted to the journal's Computational Methods in Science and Engineering section August 7, 2013; accepted for publication (in revised form) June 19, 2014; published electronically October 14, 2014. Special thanks are extended to Dr. Mujeeb Malik for funding this work as part of the "Revolutionary Computational Aerosciences" project. Sandia National Laboratories is a multiprogram laboratory managed and operated by Sandia Corporation, a wholly owned subsidiary of Lockheed Martin Corporation, for the U.S. Department of Energy's National Nuclear Security Administration under contract DE-AC04-94AL85000. This work was performed by an employee of the U.S. Government or under U.S. Government contract. The U.S. Government retains a nonexclusive, royalty-free license to publish or reproduce the published form of this contribution, or allow others to do so, for U.S. Government purposes. Copyright is owned by SIAM to the extent not limited by these rights.
http://www.siam.org/journals/sisc/36-5/93219.html

†Computational AeroSciences Branch (CASB), NASA Langley Research Center (LaRC), Hampton, VA 23681 (mark.h.carpenter@nasa.gov, eric.j.nielsen@nasa.gov).

‡Computational Thermal and Fluid Mechanics, Sandia National Labs, Albuquerque, NM 87185 (tcfishe@sandia.gov).

§School of Mechanical Engineering, Purdue University, West Lafayette, IN 47907 (stevenfrankel@purdue.edu).

alleviating instabilities.

Recent references [12, 13, 4] provide a general procedure for developing entropy conservative and entropy stable diagonal norm summation-by-parts (SBP) operators for the Navier–Stokes equations. The generalization to multidomain operators follows immediately using simultaneous-approximation-term (SAT) penalty type interface conditions [8]. The work generalizes entropy stability results appearing in the finite-volume/finite-difference literature by several authors over the past two decades [40, 41, 30, 24, 16]; an overview of the evolutionary developments is presented elsewhere [3]. Although the primary focus of references [12, 13] is entropy stable WENO finite-difference schemes, all proofs immediately generalize to any order spatial discretization that may be expressed as a nondissipative diagonal norm SBP-SAT operator [4].

Spectral collocation operators are readily expressed in SBP-SAT form [5, 22, 9, 17], although not all may be expressed as diagonal norm SBP operators; e.g., the mass matrix of a Chebyshev operator is full. Legendre collocation schemes, however, may be expressed as diagonal norm SBP operators and therefore satisfy the sufficient conditions for an entropy stable implementation.

Conservation form entropy conservative Legendre spectral collocation schemes are developed herein for the Navier–Stokes equations. An SBP-SAT developmental framework is used to motivate the development. Because this framework differs from the conventional approaches used in the spectral element and finite-element method (FEM) literature [21], the resulting schemes have some desirable properties. The SBP-SAT Legendre spectral collocation schemes are strictly conservative and entropy conservative for the Euler equations, for arbitrary order polynomials. Simultaneously satisfying mass, momentum, energy, and entropy constraints is a very desirable property. The entropy constraint enforces nonlinear neutral stability for the Euler equations—a stability datum neither dissipative nor divergent against which all other operators may be compared. The strong conservation form representation allows them to be readily extended to capture shocks via a comparison approach [41, 13].

Nonlinear entropy stability for the Navier–Stokes equations is not new. Proofs first appeared in the work of Hughes, Franca, and Mallet [23] in the context of Galerkin and Petrov–Galerkin FEMs. Stability is achieved by rotating the conservative equations into symmetric form followed by a conventional FEM implementation. The flaw in this approach is that symmetrizing the equations raises the question of whether the method is consistent with the Lax–Wendroff theorem.

Conservation form entropy stability proofs for alternative nonlinear equations appear in many finite-element texts (e.g., see Hesthaven and Warburton [21] for a discussion of the Burgers equation). A sharp extension to the compressible Navier–Stokes equations in conservation form has not been forthcoming to the best of our knowledge. Indeed, a fundamental obstacle in FEM proofs is the requirement for exact integration formulae, a feat that is all but impossible for the compressible Navier–Stokes equations. (Recasting the equations in entropy variables again raises the question of consistency with the Lax–Wendroff theorem.) The SBP-SAT Legendre entropy stability proofs do not suffer these limitations.

The entropy stable spectral collocation element (SSSCE) schemes provide an important step toward a provably stable simulation methodology of arbitrary order for complex geometries. All proofs generalize immediately to three dimensions via tensor product arithmetic, to three-dimensional (3D) curvilinear coordinates [11], and to multiple domains via an SAT penalty approach. Several major hurdles remain,

however, on the path toward complete L^2 stability of the compressible Navier–Stokes equations, including shocks.

A major difficulty is the formulation of the comparison algorithm used to capture shocks. In a comparison approach, the entropy conservative formulation is used in conjunction with a companion algorithm that is dissipative. The entropy generated by the companion scheme is compared with the entropy datum, and if the entropy condition is violated, then more dissipation is added locally. Several companion operators are considered herein (e.g., WENO, MUSCL, and strong form nodal DG) for the purpose of demonstrating the comparison approach for the SSSCE schemes. The optimal companion operator for an SSSCE scheme is still an open question and is the topic of ongoing research.

A second obstacle is the need for well-posed physical boundary conditions for the Navier–Stokes equations that preserve the entropy stability property of the interior operator. Nonlinearly stable boundary conditions for the Euler equations appear in reference [39] but do not include viscous effects. Another obstacle is the need for a temporal discretization that preserves the semidiscrete entropy stability properties (e.g., the trapezoidal rule) [41] and maintains positivity of the density and temperature. Neither boundary conditions nor temporal discretizations are addressed herein.

The organization of this paper is as follows. The theory of SBP-SAT operators and their relationship to polynomial spectral collocation formulations is presented in section 2. This discussion is tutorial in extent and may be skipped by readers familiar with SBP-SAT nomenclature and operators. Section 3 presents an introduction to continuous entropy analysis followed by semidiscrete analysis that demonstrates the entropy-mimetic properties of diagonal norm SBP operators. The analysis is valid for arbitrarily high-order accurate Legendre spectral collocation operators. Section 4 presents the SAT inviscid and viscous coupling conditions used to connect adjoining elements. Section 5 provides a discussion on the comparison approach as applied to the SSSCE schemes. Details of the implementation of entropy conservative operators in the context of the compressible Euler and Navier–Stokes equations are provided in section 6. Finally, the accuracy of the resulting high-order schemes is demonstrated in section 7, and conclusions are discussed in section 8.

2. Methodology. Consider the calorically perfect Navier–Stokes equations, which may be expressed in the form

$$\begin{aligned} q_t + (f^i)_{x_i} &= (f^{(v)i})_{x_i}, \quad x \in \Omega, \quad t \in [0,\infty), \\ Bq &= g_b, \quad x \in \partial\Omega, \quad t \in [0,\infty), \\ q(x,0) &= g_0(x), \quad x \in \Omega, \end{aligned} \tag{2.1}$$

where the Cartesian coordinates, $x = (x_1, x_2, x_3)^T$, and time, t, are independent variables, and index sums are implied. The vectors q, f^i, and $f^{(v)i}$ are the conserved variables, the conserved inviscid fluxes, and the viscous fluxes, respectively. Without loss of generality, a 3D box

$$\Omega = [x_1^L, x_1^H] \times [x_2^L, x_2^H] \times [x_3^L, x_3^H]$$

is chosen as our physical domain with $\partial\Omega$ representing the boundary of the domain. The boundary vector, g_b, is assumed to contain well-posed Dirichlet/Neumann data. We have omitted a detailed description of the 3D Navier–Stokes equations, which may be found elsewhere [11].

The physical domain is divided into subdomains (elements). The Navier–Stokes equations are then discretized on each element using an entropy stable spectral collocation method; details of the semidiscrete operators are included in sections 2 and 3. Adjoining elements are then coupled in a conservative and design order fashion, while preserving an entropy estimate across the interface; details are provided in section 4. The analysis and simulations presented herein assume variable size Cartesian elements.

2.1. Summation-by-parts operators.

2.1.1. First derivative. First derivative operators that satisfy the SBP convention discretely mimic the integration-by-parts condition

$$\int_{x_L}^{x_R} \phi q_x \,\mathrm{d}x = \phi q|_{x_L}^{x_R} - \int_{x_L}^{x_R} \phi_x q \,\mathrm{d}x. \tag{2.2}$$

This mimetic property is achieved by constructing the first derivative approximation, $\mathcal{D}\boldsymbol{\phi}$, with an operator in the form

$$\begin{gathered} \mathcal{D} = \mathcal{P}^{-1}\,\mathcal{Q}, \quad \mathcal{P} = \mathcal{P}^T, \quad \boldsymbol{\zeta}^T \mathcal{P} \boldsymbol{\zeta} > 0, \quad \boldsymbol{\zeta} \neq \mathbf{0}, \\ \mathcal{Q}^T = \mathcal{B} - \mathcal{Q}, \quad \mathcal{B} = \mathrm{diag}\,(-1, 0, \ldots, 0, 1)\,. \end{gathered} \tag{2.3}$$

While it is not true in general that $\mathcal{P}$ is diagonal, herein the focus is exclusively on diagonal norm SBP operators based on fixed element-based polynomials. The matrix $\mathcal{P}$ may be thought of as a mass matrix in the context of Galerkin finite elements and incorporates the local grid spacing into the derivative definition. The nearly skew-symmetric matrix, $\mathcal{Q}$, is an undivided differencing operator where all rows sum to zero and the first and last columns sum to -1 and 1, respectively. The accuracy of the first derivative operator, $\mathcal{D}$, may be expressed as

$$\phi_x(\mathbf{x}) = \mathcal{D}\boldsymbol{\phi} + \mathcal{T}_{(p+1)}, \quad \boldsymbol{\phi} = \left(\phi(x_1), \phi(x_2), \ldots, \phi(x_N)\right)^T\,, \tag{2.4}$$

where $\mathcal{T}_{(p+1)}$ is the truncation error of the approximation, and p is the order of the polynomial. Integration in the approximation space is conducted using an inner product with the appropriate integration weights provided by the norm $\mathcal{P}$,

$$\int_{x_L}^{x_R} \phi q_x \,\mathrm{d}x \approx \boldsymbol{\phi}^T \mathcal{P} \mathcal{D} \mathbf{q}, \quad \mathbf{q} = \left(q(x_1), q(x_2), \ldots, q(x_N)\right)^T. \tag{2.5}$$

Using the definitions provided in (2.3), the SBP property is demonstrated:

$$\boldsymbol{\phi}^T \mathcal{P} \mathcal{P}^{-1} \mathcal{Q} \mathbf{q} = \boldsymbol{\phi}^T \left(\mathcal{B} - \mathcal{Q}^T\right) \mathbf{q} = \phi_N q_N - \phi_1 q_1 - \boldsymbol{\phi}^{\boldsymbol{T}} \mathcal{D}^T \mathcal{P} \mathbf{q}. \tag{2.6}$$

Note that in (2.6) the action of the discrete derivative is transferred directly onto the test function with an equivalent order of approximation.

The specific operators used in this work are presented elsewhere [3].

2.1.2. The second derivative. The viscous approximations are written in general as

$$\left(\vartheta(x) q_x(\mathbf{x})\right)_x = \mathcal{D}_2(\vartheta)\mathbf{q} + \mathcal{T}_p^{(v)} \tag{2.7}$$

and also satisfy the SBP condition. Integration by parts yields

$$\int_{x_L}^{x_R} \phi \left(\vartheta q_x\right)_x \,\mathrm{d}x = \phi \vartheta q_x|_{x_L}^{x_R} - \int_{x_L}^{x_R} \phi_x \vartheta q_x \,\mathrm{d}x. \tag{2.8}$$

The second derivative variable coefficient operator resulting from two applications of the first derivative may be manipulated for diagonal norm, $\mathcal{P}$, into the expression

(2.9)
$$\mathcal{D}_2(\vartheta) = \mathcal{P}^{-1}\left(-\mathcal{D}^T\mathcal{P}[\vartheta]\mathcal{D} + \mathcal{B}[\vartheta]\mathcal{D}\right), \quad \mathcal{D}^T\mathcal{P}[\vartheta]\mathcal{D} = \left(\mathcal{D}^T\mathcal{P}[\vartheta]\mathcal{D}\right)^T, \quad [\vartheta] = \mathrm{diag}\left(\vartheta(\mathbf{x})\right),$$
$$\boldsymbol{\zeta}^T\left(\mathcal{D}^T\mathcal{P}[\vartheta]\mathcal{D}\right)\boldsymbol{\zeta} \geq 0, \quad \boldsymbol{\zeta}^T[\vartheta]\boldsymbol{\zeta} \geq 0 \quad \forall \boldsymbol{\zeta}.$$

The $\mathcal{P}$-norm inner product yields the expression

$$\boldsymbol{\phi}^T\mathcal{P}\mathcal{P}^{-1}\left(-\mathcal{D}^T\mathcal{P}[\vartheta]\mathcal{D} + \mathcal{B}[\vartheta]\mathcal{D}\right)\mathbf{q} = \boldsymbol{\phi}^T\mathcal{B}[\vartheta]\mathcal{D}\mathbf{q} - \boldsymbol{\phi}^T\left(\mathcal{D}^T\mathcal{P}[\vartheta]\mathcal{D}\right)\mathbf{q}, \tag{2.10}$$

which is the form used to show stability of the viscous terms. It is clear that the continuous interface terms are mimicked. Likewise, based on the definition (2.9), the expression

$$\int_{x_L}^{x_R} \phi_x \vartheta q_x \,\mathrm{d}x \approx \boldsymbol{\phi}^T\left(\mathcal{D}^T\mathcal{P}[\vartheta]\mathcal{D}\right)\mathbf{q}$$

follows immediately.

2.1.3. Complementary grids. Most existing entropy analysis is performed in indicial notation on a staggered set of solution and flux points. For example, Tadmor's telescopic entropy flux relation (fully defined in section 3.2.2) is written as

$$\left(w_{i+1} - w_i\right)^T \bar{f}_i = \psi_{i+1} - \psi_i$$

and relates solution point data $w_i, w_{i+1}, \psi_i, \psi_{i+1}$ with a flux $\bar{f}_i$ located between the grid points. Conventional SBP operators are not directly applicable to this form of analysis; generalized operators suitable for a staggered grid implementation are now developed. The complementary grids and their properties are defined in this subsection. In subsection 2.1.4 it is shown that SBP operators satisfy a generalized SBP property on the complementary grids.

Define on the interval $-1 \leq x \leq 1$ the vectors of discrete solution points

$$\mathbf{x} = \left[x_1, x_2, \ldots, x_{N-1}, x_N\right]^T \quad ; \quad -1 \leq x_1, x_2, \ldots, x_{N-1}, x_N \leq 1\,. \tag{2.11}$$

Since the approximate solution is constructed at these points, they are denoted the *solution points*. It is useful to create a set of $(N+1)$ intermediate points $\bar{\mathbf{x}}$ defining control volume bounds around each solution point. These points are denoted *flux points* as they are similar in nature to the control volume edges employed in the finite-volume method. The distribution of the flux points depends on the discretization operator $\mathcal{D} = \mathcal{P}^{-1}\mathcal{Q}$. The spacing between the flux points is implicitly defined by the norm $\mathcal{P}$; the diagonal elements of $\mathcal{P}$ are equal to the spacing between flux points,

$$\begin{gathered}\bar{\mathbf{x}} = \left(\bar{x}_0, \bar{x}_1, \ldots, \bar{x}_N\right)^T, \quad \bar{x}_0 = x_1, \quad \bar{x}_N = x_N, \\ \bar{x}_i - \bar{x}_{i-1} = \mathcal{P}_{(i)(i)}, \quad i = 1, 2, \ldots, N.\end{gathered} \tag{2.12}$$

In operator notation, this is equivalent to

$$\Delta\bar{\mathbf{x}} = \mathcal{P}\mathbf{1} \quad ; \quad \mathbf{1} = (1, 1, \ldots, 1)^T, \tag{2.13}$$

where the $N \times (N+1)$ matrix Δ is defined as

$$\Delta = \begin{pmatrix} -1 & 1 & 0 & 0 & 0 & 0 \\ 0 & -1 & 1 & 0 & 0 & 0 \\ 0 & 0 & \ddots & \ddots & 0 & 0 \\ 0 & 0 & 0 & -1 & 1 & 0 \\ 0 & 0 & 0 & 0 & -1 & 1 \end{pmatrix} \tag{2.14}$$

and calculates the undivided difference of the two adjacent flux points.

Note that in (2.12), the first and last flux points are coincident with the first and last solution points. This fact enables the endpoint fluxes to be consistent:

$$\bar{f}_0 = f(q_1), \quad \bar{f}_N = f(q_N). \tag{2.15}$$

This duality is needed to define unique operators and is important in proving entropy stability.

Remark. The introduction of complementary grids makes nomenclature significantly more challenging. Herein, all vectors are represented in bold font, while matrices (when possible) are represented using calligraphic font. The "over-bar" symbol is reserved for flux point vectors; the $N+1$ dimensional flux point vectors are numbered from $0 \le i \le N$. In general, matrix ranks are inferred by the dimension of the vectors on which they operate. If the rank of a matrix or vector is ambiguous, then the rank is provided in the text.

2.1.4. Telescopic flux form. Reference [14] proves that any SBP matrix $\mathcal{Q}$ can be expressed as $\mathcal{Q} = \Delta\, {}_{(N+1)}I_n$: the product of the $N \times (N+1)$ difference operator Δ and a unique $(N+1) \times N$ interpolation operator ${}_{(N+1)}I_n$. Thus, all SBP derivative operators $\mathcal{D} = \mathcal{P}^{-1}\mathcal{Q}$ can be manipulated into the telescopic flux form,

$$f_x(\mathbf{q}) = \mathcal{P}^{-1}\mathcal{Q}\mathbf{f} + \mathcal{T}_{(p+1)} = \mathcal{P}^{-1}\Delta\overline{\mathbf{f}} + \mathcal{T}_{(p+1)} \tag{2.16}$$

with $\overline{\mathbf{f}} = {}_{(N+1)}I_n\, \mathbf{f}$. Conservation follows immediately for telescopic derivative operators in the form of (2.16). The following lemma reiterates this telescopic property of all SBP operators. (The original proof appears in reference [14].)

LEMMA 2.1. *All differentiation matrices that satisfy the SBP convention given in* (2.3) *are telescopic operators in the norm* $\mathcal{P}$ *and the difference operator* Δ.

This telescopic flux form of $\mathcal{D}$ motivates a generalized SBP property. (See (2.34) for the conventional SBP property.) The telescopic flux form defined in (2.16) combined with the flux consistency condition results in a more generalized relation,

$$\boldsymbol{\phi}^T\mathcal{P}\mathcal{P}^{-1}\Delta\overline{\mathbf{f}} = \boldsymbol{\phi}^T(\tilde{\mathcal{B}} - \tilde{\Delta})\overline{\mathbf{f}} = f(q_N)\phi_N - f(q_1)\phi_1 - \boldsymbol{\phi}^T\tilde{\Delta}\overline{\mathbf{f}}, \tag{2.17}$$

where

$$\tilde{\Delta} = \begin{pmatrix} 0 & -1 & 0 & 0 & 0 & 0 \\ 0 & 1 & -1 & 0 & 0 & 0 \\ 0 & 0 & \ddots & \ddots & 0 & 0 \\ 0 & 0 & 0 & 1 & -1 & 0 \\ 0 & 0 & 0 & 0 & 1 & 0 \end{pmatrix}, \quad \tilde{\mathcal{B}} = \begin{pmatrix} -1 & 0 & 0 & 0 & 0 & 0 \\ 0 & 0 & 0 & 0 & 0 & 0 \\ 0 & 0 & \ddots & \ddots & 0 & 0 \\ 0 & 0 & 0 & 0 & 0 & 0 \\ 0 & 0 & 0 & 0 & 0 & 1 \end{pmatrix},$$

and

$$\frac{1}{\delta x}\boldsymbol{\phi}^T\tilde{\Delta} = \boldsymbol{\phi}_x^T + \mathcal{O}(\delta x)$$

with δx an average distance between collocation points.

This is equivalent to the commonly used explanation of SBP in indicial form,

$$\sum_{i=1}^{N} \phi_i \left(\bar{f}_i - \bar{f}_{i-1}\right) = f(q_N)\phi_N - f(q_1)\phi_1 - \sum_{i=1}^{N-1} \bar{f}_i \left(\phi_{i+1} - \phi_i\right). \tag{2.18}$$

Like the conventional SBP operator, the action of the derivative is moved onto the test function. However, the test function derivative is only first-order accurate. This generalized SBP property is used herein to construct entropy conservative fluxes and is also instrumental for satisfying the Lax–Wendroff theorem [28] in weak form.

Likewise, the variable coefficient viscous operators presented in section 2.1.2 may be expressed in the form

$$(\vartheta q_x(\mathbf{x}))_x \approx \mathcal{P}^{-1}\left(-\mathcal{D}^T\mathcal{P}[\vartheta]\mathcal{D} + \mathcal{B}[\vartheta]\mathcal{D}\right)\mathbf{q} = \mathcal{P}^{-1}\Delta\overline{\mathbf{f}}^{(v)} \tag{2.19}$$

and satisfy a telescopic conservation property which is identical to that of the inviscid terms.

2.1.5. The semidiscrete operator. Based on the previous discussion of SBP operators and their equivalent telescopic form, the semidiscrete form of (2.1) becomes

$$\mathbf{q}_t = -\mathcal{D}_i[\mathbf{f}^i(v)] + \mathcal{D}_i[c]_{ij}\mathcal{D}_j\mathbf{q} + \mathcal{P}^{-1}(\mathbf{g}_b + \mathbf{g}_i) = \mathcal{P}^{-1}\Delta_i\left(-\overline{\mathbf{f}}^i + \overline{\mathbf{f}}^{(v)i}\right) + \mathcal{P}^{-1}(\mathbf{g}_b + \mathbf{g}_i), \tag{2.20}$$

$$\mathbf{q}(x,0) = g_0(x), \quad x \in \Omega,$$

with $\mathbf{g}_b$ and $\mathbf{g}_i$ enforcing of physical boundary conditions and element-element interface conditions, respectively. Full implementation details of the interior operators, including the viscous Jacobian $[c]_{ij}$ tensors, are included in previous works [14, 15]. Both $\mathbf{g}_b$ and $\mathbf{g}_i$ are constructed using a penalty approach. Specific details on the construction of boundary $\mathbf{g}_b$ and interface $\mathbf{g}_i$ penalty terms are given in subsection 2.4 and in section 4, respectively.

2.2. Spectral discretization operators. Spectral collocation methods are commonly implemented on computational grids based on the nodes of Gauss quadrature formulas (i.e., Gauss, Gauss–Radau, or Gauss–Lobatto (GL)).

The numerical methods developed herein are all collocated at the Legendre GL (LGL) points and include both endpoints of the interval. Including the endpoints in the grid distribution allows the operators to be written in terms of flux differences, analogous to a finite-volume method and consistent with (2.17) and (2.19). The complete discretization operator for the $p = 4$ element is illustrated in Figure 1.

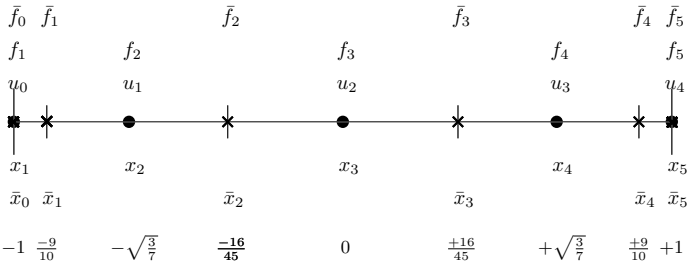

FIG. 1. *The one-dimensional discretization for $p = 4$ Legendre collocation is illustrated. Solution points are denoted by $\bullet$ and flux points are denoted by $\times$.*

2.2.1. Lagrange polynomials. Define the Lagrange polynomials on the discrete points $\mathbf{x}$ as

$$L_j(x) = \prod_{\substack{k=1 \\ k\neq j}}^{N} \frac{x - x_k}{x_j - x_k}, \qquad 1 \le j \le N. \tag{2.21}$$

With a slight abuse of notation, define the *vector* of Lagrange polynomials as

$$\mathbf{L}(x) \quad = \quad [L_1(x), L_2(x), \ldots, L_{N-1}(x), L_N(x)]^T. \tag{2.22}$$

2.3. Differentiation. Assume that a smooth and (infinitely) differentiable function, $f(x)$, is defined on the interval $-1 \leq x \leq 1$. Reading the function f and derivative f' at the discrete points, $\mathbf{x}$, yields the vectors

$$\begin{array}{rcl} \mathbf{f}(\mathbf{x}) & = & [f(x_1), f(x_2), \ldots, f(x_{N-1}), f(x_N)]^T; \\ \mathbf{f}'(\mathbf{x}) & = & [f'(x_1), f'(x_2), \ldots, f'(x_{N-1}), f'(x_N)]^T. \end{array} \tag{2.23}$$

The interpolation polynomial, $f_N(x)$, that collocates $f(x)$ at the points $\mathbf{x}$ is given by the contraction

$$f(x) \;\approx\; f_{(N-1)}(x) \;=\; [\mathbf{L}(x)]^T \mathbf{f}(\mathbf{x})\,. \tag{2.24}$$

Derivative operators expressed in terms of the Lagrange polynomials on the interval are derived in the following theorem, presented without proof. (The proof appears in many texts, e.g., reference [26].)

THEOREM 2.2. *The derivative operator that exactly differentiates an arbitrary nth order polynomial at the collocation points,* $\mathbf{x}$*, is*

$$\mathcal{D} \;=\; [L_j^{'}(x_i)]\,. \tag{2.25}$$

The elements of $\mathcal{D}$ *are* $d_{i,j}$ *for* $1 \leq i,\, j \leq p$.

An equivalent representation of the differentiation operator may also be used; it satisfies all the requirements for being an SBP operator (but in general will not be a diagonal norm SBP operator).

THEOREM 2.3. *The derivative operator that exactly differentiates an arbitrary pth order polynomial* ($p = N-1$) *at the collocation points,* $\mathbf{x}$*, may be expressed as*

$$\mathcal{D} \;=\; \mathcal{P}^{-1}\, \mathcal{Q}\,. \tag{2.26}$$

Proof. First note that in addition to (2.33), the exact derivative $\frac{df(x)}{dx}$ of the function $f(x)$ may be approximated by

$$f'(x) \;\approx\; \frac{df_n(x)}{dx} \;=\; [\mathbf{L}(x)]^T \mathbf{f}'(\mathbf{x})\,. \tag{2.27}$$

The Galerkin statement demands that the integral error between the two expressions be orthogonal to the basis set which in this case is the Lagrange polynomials $\mathbf{L}(x)$. This statement may be expressed as

$$\int_{-1}^{1} \mathbf{L}(x) \left([\mathbf{L}(x)]^T \mathbf{f}'(\mathbf{x}) \;-\; [\mathbf{L}^{'}(x)]^T \mathbf{f}(\mathbf{x}) \right)\, dx \;=\; 0\,, \tag{2.28}$$

or in the equivalent form

$$\hat{\mathcal{P}}\, \mathbf{f}'(\mathbf{x}) \;=\; \mathcal{Q}\, \mathbf{f}(\mathbf{x})\,, \tag{2.29}$$

with

$$\hat{\mathcal{P}} \;=\; \textstyle\int_{-1}^{1} \mathbf{L}(x)[\mathbf{L}(x)]^T\, dx \qquad ; \qquad \mathcal{Q} \;=\; \int_{-1}^{1} \mathbf{L}(x)[\mathbf{L}^{'}(x)]^T\, dx\,. \tag{2.30}$$

Equation (2.26) follows immediately when $\hat{\mathcal{P}}$ is symmetric positive definite (SPD) and therefore invertible.

The symmetry of $\hat{\mathcal{P}}$ follows immediately from definition (2.30). Positive definiteness of $\hat{\mathcal{P}}$ is established by pre- and postmultiplying $\hat{\mathcal{P}}$ by an arbitrary nonzero discrete vector, ψ, which yields the expression

$$\psi^T \hat{\mathcal{P}} \psi \;=\; \int_{-1}^{1} \psi^T \mathbf{L}(x)[\mathbf{L}(x)]^T \psi \, dx \;=\; \int_{-1}^{1} \psi(x)^2 \, dx, \tag{2.31}$$

which is strictly greater than zero unless ψ is the null vector. Thus, the matrix $\hat{\mathcal{P}}$ is SPD and therefore invertible, and (2.26) follows immediately. ∎

A proof that $\mathcal{Q}$ is nearly skew-symmetric is as follows.

THEOREM 2.4. *The matrix* $\mathcal{Q} = \int_{-1}^{1} \mathbf{L}(x)[\mathbf{L}'(x)]^T dx$ *is structurally of the form*

$$\mathcal{Q} + \mathcal{Q}^T = \mathcal{B}\,. \tag{2.32}$$

Thus, by virtue of the structure of $\hat{\mathcal{P}}$ and $\mathcal{Q}$, the differentiation operator, $\mathcal{D}$, is indeed an SBP operator defined by (2.3).

Proof. Integrating by parts the definition of $\mathcal{Q}$ yields the expression

$$\mathcal{Q} = \int_{-1}^{1} \mathbf{L}(x)[\mathbf{L}'(x)]^T dx = \mathbf{L}(x)(+1)[\mathbf{L}(x)(+1)]^T - \mathbf{L}(x)(-1)[\mathbf{L}(x)(-1)]^T - \int_{-1}^{1} \mathbf{L}'(x)[\mathbf{L}(x)]^T dx. \tag{2.33}$$

All Lagrange polynomials based on the GL collocation points vanish on the boundaries for $1 < i, j < N$. Thus, the boundary matrices reduce to the form

$$\mathbf{L}(+1)[\mathbf{L}(+1)]^T - \mathbf{L}(-1)[\mathbf{L}(-1)]^T \;=\; \delta_{i,N}\delta_{j,N} - \delta_{i,1}\delta_{j,1}.$$

Writing (2.33) in indicial nomenclature leads to $q_{i,j} + q_{j,i} = \delta_{i,N}\delta_{j,N} - \delta_{i,1}\delta_{j,1}$, which is the desired result. ∎

2.3.1. Collocation. A Legendre collocation operator may be constructed by approximating the integrals in (2.30), (2.31), and (2.4) by the LGL quadrature formula. Let $\eta = (\eta_1, \eta_2, \ldots, \eta_{N-1}, \eta_N)$ be the nodes of the LGL quadrature formula (i.e., the zeros of the polynomial $P'_{n-1}(x)(1-x^2)$ [26]), and let ω_l, $1 \le l \le N$, be the quadrature weights. Define $\mathbf{L}(\eta_l; \mathbf{x})$ as the vector of Lagrange polynomials $\mathbf{L}(x)$ evaluated at the quadrature point η_l; i.e.,

$$\mathbf{L}(\eta_l; \mathbf{x}) \;=\; [L_1(\eta_l), L_2(\eta_l), \ldots, L_N(\eta_l)]^T.$$

Using these definitions, the mass and stiffness matrices $\mathcal{P}$ and $\mathcal{Q}_c$ are given by the expressions

$$\mathcal{P} \;=\; \textstyle\sum_l \mathbf{L}(\eta_l; \mathbf{x})[\mathbf{L}(\eta_l; \mathbf{x})]^T \omega_l \qquad ; \qquad \mathcal{Q}_c \;=\; \sum_l \mathbf{L}(\eta_l; \mathbf{x})[\mathbf{L}'(\eta_l; \mathbf{x})]^T \omega_l \;. \tag{2.34}$$

The matrix $\mathcal{P}$ is SPD for any $\mathbf{x}$ [5].

Note that, in general, $\hat{\mathcal{P}} \neq \mathcal{P}$. The LGL formula is exact for polynomials of degree $2p-1$, but $\int_{-1}^{1} \mathbf{L}(x)[\mathbf{L}(x)]^T \, dx$ is of degree $2p$. Thus, the integration differs for the highest-order term (i.e., the $2p$th). Indeed, the two matrix norms differ by a rank one perturbation, i.e., $\hat{\mathcal{P}} = \mathcal{P} + \gamma_p \mathcal{D}^p \mathbf{e_0}[\mathcal{D}^p \mathbf{e_0}]^T$, where $\mathbf{e_0} = [1, 0, \ldots, 0]^T$, $\mathcal{D}^p$ is the highest derivative supported by the polynomial, and γ_p depends on polynomial order.

The matrices $\mathcal{Q}$ and $\mathcal{Q}_c$ are equivalent. This follows from the fact that the two matrices are defined by the polynomials $\int_{-1}^{1} \mathbf{L}(x)[\mathbf{L}'(x)]^T\, dx$ that have a combined rank of $2p-1$. Therefore, integration is exact when using the LGL integration formula.

The uniqueness of the differentiation matrix $\mathcal{D}$ yields the expression

$$\mathcal{D} = \hat{\mathcal{P}}^{-1}\mathcal{Q} = \mathcal{P}^{-1}\mathcal{Q}\,.$$

This statement does not contradict the fact that $\hat{\mathcal{P}} \neq \mathcal{P}$. Indeed, it can be shown using the Sherman–Morrison formula that the difference (i.e., $\hat{\mathcal{P}}^{-1} - \mathcal{P}^{-1}$) lies in the null space of the singular $\mathcal{Q}$ matrix.

2.3.2. Diagonal norm SBP operators.

THEOREM 2.5. *The matrix $\mathcal{P}$ is diagonal for collocation points located at the LGL quadrature points, i.e., $\mathbf{x} = \eta$. Furthermore, the diagonal coefficients of $\mathcal{P}$ are the integration weights ω_l, $1 \leq l \leq N$, used in the quadrature.*

Proof. Recall that the Lagrange polynomials evaluated at the knot points satisfy the property $L_i(x_j) = \delta_{i,j}$. Thus, the result follows immediately from the definition of the norm $\mathcal{P} = \sum_l \mathbf{L}(\eta_l;\mathbf{x})[\mathbf{L}(\eta_l;\mathbf{x})]^T\omega_l$. ∎

2.4. SAT penalty boundary and interface conditions. Physical boundary conditions and coupling conditions between adjoining elements greatly influence the stability and accuracy of the solution. A straightforward method that permits formal analysis is the SAT penalty method. The SAT method solves the governing equation on the boundary (interface) and simultaneously penalizes the numerical solution against well-posed physical (interface) data. This technique is design order accurate provided the solution is penalized against accurate data and can be used to design conservative boundary (interface) conditions that are provably stable. General construction and implementation details of penalty type boundary conditions can be found in [6]. A full description of the boundary conditions that are designed specifically for the Navier–Stokes equations can be found in [38, 37, 34, 2].

Remark. The test problems studied herein are limited to open boundaries. The numerical SAT boundary conditions are based on the linear analysis of Svärd, Carpenter, and Nordström [37] and are enforced via the term $\mathbf{g}_b$ in (2.20). Boundary conditions that preserve the nonlinear entropy stability of the interior operator are currently not available (to the best of our knowledge) for the Navier–Stokes equations.

3. Entropy stable spectral collocation: Single domain.

3.1. Continuous analysis.

3.1.1. Smooth solutions. Consider a nonlinear system of equations (e.g., the Navier–Stokes equations given in (2.1)), and assume that the solution is smooth for all time. The objective is to bound the solution as sharply as possible. A quadratic or otherwise convex extension of the original equations is sought, that when integrated over the domain depends only on boundary data and dissipative terms. The convex extension for the Navier–Stokes equations is the entropy function and provides a mechanism for proving stability of the nonlinear system.

DEFINITION 3.1. *A scalar function $S = S(q)$ is an entropy function of* (2.1) *if it satisfies the following conditions:*

- *The function $S(q)$ is convex and, when differentiated, simultaneously contracts all spatial fluxes as follows:*

$$S_q f^i_{x_i} = S_q f^i_q q_{x_i} = F^i_q q_{x_i} = F^i_{x_i} \quad ; \quad i = 1, \ldots, d, \tag{3.1}$$

for each spatial coordinate, d. The components of the contracting vector, S_q, are the entropy variables denoted as $w^T = S_q$. $F^i(q)$ are the entropy fluxes in the i-direction.

- *The entropy variables, w, symmetrize* (2.1) *if w assumes the role of a new dependent variable (i.e., $q = q(w)$). Expressing* (2.1) *in terms of w is*

(3.2)
$$q_t + (f^i)_{x_i} - (f^{(v)i})_{x_i} = q_w w_t + (f^i_w) w_{x_i} - (\hat{c}_{ij} w_{x_j})_{x_i} = 0 \quad ; \quad i = 1, \ldots, d,$$

with the symmetry conditions $q_w = [q_w]^T$, $f^i_w = f^{i\,T}_w$, $\hat{c}_{ij} = \hat{c}^T_{ji}$.

Because the entropy is convex, the Hessian $S_{qq} = w_q$ is SPD,

$$\zeta^T S_{qq} \zeta > 0 \quad \forall \zeta \neq 0, \tag{3.3}$$

and yields a one-to-one mapping from conservation variables, q, to entropy variables, $w^T = S_q$. Likewise, w_q is SPD because $q_w = {w_q}^{-1}$ and SPD matrices are invertible. The entropy and corresponding entropy flux are often denoted an entropy–entropy flux pair, (S, F). Likewise, the potential and the corresponding potential flux (defined next) are denoted a potential–potential flux pair, (φ, ψ) [41].

The symmetry of the matrices q_w and f^i_w indicates that the conservation variables, q, and fluxes, f^i, are Jacobians of scalar functions with respect to the entropy variables,

$$q^T = \varphi_w, \quad [f^i]^T = \psi^i_w, \tag{3.4}$$

where the nonlinear function, φ, is called the potential and ψ^i are called the potential fluxes [41]. Just as the entropy function is convex with respect to the conservative variables (S_{qq} is positive definite), the potential function is convex with respect to the entropy variables.

The two elements of Definition 3.1 are closely related, as is shown by Godunov [18] and Mock [33]. Godunov proves the following theorem.

THEOREM 3.2. *If* (2.1) *can be symmetrized by introducing new variables w, and w is a convex function of φ, then an entropy function $S(q)$ is given by*

$$\varphi = w^T q - S, \tag{3.5}$$

and the entropy fluxes $F^i(q)$ satisfy

$$\psi^i = w^T f^i - F^i. \tag{3.6}$$

Mock proves the converse to be true.

THEOREM 3.3. *If $S(q)$ is an entropy function of* (2.1)*, then $w^T = S_q$ symmetrizes the equation.*

See reference [19] for a detailed summary of both proofs.

Entropy stability analysis is now performed on the Navier–Stokes equations. Contracting (2.1) with the entropy variables forms the convex extension; the differential form of the entropy equation is

(3.7)
$$S_q q_t + S_q f(q)_{x_i} = S_t + F_{x_i} = S_q f^{(v)}_{x_i} = \left(w^T f^{(v)}\right)_{x_i} - w^T_{x_i} f^{(v)i} = \left(w^T f^{(v)}\right)_{x_i} - w^T_{x_i} \hat{c}_{ij} w_{x_i}.$$

Integrating (3.7) over the domain yields a global conservation statement for the entropy in the domain

$$\frac{d}{dt} \int_\Omega S \, \mathrm{d}x_i = \left[w^T f^{(v)} - F \right]_{\partial\Omega} - \int_\Omega w^T_{x_j} \hat{c}_{ij} w_{x_i} \, \mathrm{d}x_i. \tag{3.8}$$

It is shown elsewhere [12, 13] that the second integral term in the entropy equation (3.8) accounts for viscous dissipation and is always negative. Thus, the entropy equation is the convex extension of the original Navier–Stokes equations and serves as an integral measure of stability of the system.

3.1.2. Discontinuous solutions. The Euler terms in (2.1) (the convective terms to the left of the equal sign) admit discontinuous solutions in finite time even for smooth initial and boundary data. Thus, weak solutions to the integral form of (2.1) are appropriate for these situations. Although (3.8) is an integral statement of entropy conservation, it is not strictly valid in the presence of discontinuities, because it does not accurately account for the dissipation of entropy at the discontinuity (i.e., shocks).[1] Although the precise amount of entropy dissipated at a shock is not known a priori, what is known is the sign of the jump in entropy. Thus, a general (though not sharp) statement of the conservation of entropy in the domain is

$$\frac{d}{dt}\int_\Omega S\,\mathrm{d}x_i \;\le\; \Big[w^T f^{(v)} - F\Big]_{\partial\Omega} - \int_\Omega w_{x_j}^T \hat{c}_{ij} w_{x_i}\,\mathrm{d}x_i. \tag{3.9}$$

Weak solutions in general may not be unique [28, 29]. In these cases, (3.9) is available to identify spurious solutions that violate the entropy condition from those that are physically admissible.

3.2. Semidiscrete entropy analysis. The semidiscrete entropy estimate is achieved by mimicking term by term the continuous estimate given in (3.8). The nonlinear analysis begins by contracting the entropy variables, $\mathbf{w}^T$, with the semidiscrete equation (2.20). (For clarity of presentation, but without loss of generality, the derivation is simplified to one spatial dimension. Tensor product algebra allows the results to extend directly to three dimensions.) The resulting global equation that governs the semidiscrete decay of entropy is given by

$$\mathbf{w}^T\mathcal{P}\mathbf{q}_t + \mathbf{w}^T\Delta\overline{\mathbf{f}} = \mathbf{w}^T\Delta\overline{\mathbf{f}}^{(v)} + \mathbf{w}^T(\mathbf{g}_b + \mathbf{g}_i), \tag{3.10}$$

where

$$\mathbf{w} = \left(w(q_1)^T, w(q_2)^T, \ldots, w(q_N)^T\right)^T,$$

the vector of entropy variables. The semidiscrete terms are now analyzed to demonstrate that they mimic the corresponding term in the continuous entropy estimate, provided that a diagonal norm SBP operator is used. The analysis of the interface penalty terms $\mathbf{g}_i$ is presented in section 4. Recall that the boundary terms $\mathbf{g}_b$ are linear and thus are outside the scope of the entropy analysis presented herein.

3.2.1. Time derivative. The time derivative is in mimetic form for diagonal norm SBP operators. The entropy variables are defined by the expression $w^T = S_q$, which when combined with the definition of entropy yields the pointwise expression

$$w_i^T(q_i)_t \;=\; (S_i)_{q_i}(q_i)_t \;=\; (S_i)_t \quad \forall i.$$

Now, define the diagonal matrices $\mathbf{S_q} = \mathbf{W} = Diag[\mathbf{w}]$. Since $\mathcal{P}$ is a diagonal matrix and arbitrary diagonal matrices commute, the semidiscrete rate of change of entropy becomes

$$\mathbf{w}^T\mathcal{P}\mathbf{q}_t \;=\; \mathbf{1}^T\mathbf{W}\mathcal{P}\mathbf{q}_t \;=\; \mathbf{1}^T\mathcal{P}\mathbf{W}\mathbf{q}_t \;=\; \mathbf{1}^T\mathcal{P}\mathbf{S_q}\mathbf{q}_t \;=\; \mathbf{1}^T\mathcal{P}\mathbf{S}_t.$$

[1] Note that mathematical entropy has the opposite sign from thermodynamic entropy in gas dynamics.

3.2.2. Inviscid flux conditions. The inviscid portion of (3.10) is entropy conservative if it satisfies

$$\mathbf{w}^T \Delta \overline{\mathbf{f}} = F(q_N) - F(q_1) = \mathbf{1}^T \Delta \overline{\mathbf{F}}. \tag{3.11}$$

Recall that $\mathbf{w}$ and $\overline{\mathbf{f}}, \overline{\mathbf{F}}$ are defined at the solution points and flux points, respectively. Tadmor [41] developed a pointwise relation between adjoining solution and flux-point data that satisfies (3.11); the relation is given by the expression

$$(w_{i+1} - w_i)^T \bar{f}_i = \psi_{i+1} - \psi_i.$$

Entropy conservative fluxes that satisfy this two-point shuffle relationship telescope across the domain when contracted against the entropy variables, leaving only entropy fluxes on the boundaries. This relationship was developed for second-order centered operators.

A general strategy for constructing entropy conservative fluxes for high-order SBP operators is presented in [12, 13, 3]. The proofs of this general approach for building entropy conservative operators of any order are quite involved. For brevity only the three essential theorems are included herein.

A general expression that satisfies a pointwise telescopic property similar to Tadmor's entropy flux relation is summarized in the following theorem.

THEOREM 3.4. *The local conditions*

$$(w_{i+1} - w_i)^T \bar{f}_i = \tilde{\psi}_{i+1} - \tilde{\psi}_i, \quad i = 1, 2, \ldots, N-1 \quad ; \quad \tilde{\psi}_1 = \psi_1, \quad \tilde{\psi}_N = \psi_N, \tag{3.12}$$

when summed, telescope across the domain and satisfy the entropy conservative condition given in (3.11)*. A flux that satisfies this condition given in* (3.12) *is denoted* $\bar{f}_i^{(S)}$*. The potentials* $\tilde{\psi}_{i+1}$ *and* $\tilde{\psi}_i$ *need not be the pointwise* ψ_{i+1} *and* ψ_i*, respectively.*

Proof. See Theorem 3.3 in [3] for the proof of this theorem. ∎

Note that although Theorem 3.4 provides a functional constraint for the generalized entropy flux $\bar{f}_i^{(S)}$, it provides no insight on how to construct the flux or the flux potentials.

A critical observation on how to construct $\bar{f}_i^{(S)}$ appears in [13]. The generalized entropy conservative flux $\bar{f}_i^{(S)}$ may be constructed from linear combinations of two-point entropy conservative fluxes, combined using the coefficients in the SBP matrix $\mathcal{Q}$. Because it requires only the existence of a two-point entropy conservative flux formula and the coefficients of the $\mathcal{Q}$, it is valid for any SBP operator which satisfies the constraints given in (2.3). Thus, it is valid for Legendre spectral collocation operators.

The next theorem establishes that the generalized entropy flux $\bar{f}_i^{(S)}$ constructed from a linear combination of two-point entropy conservative fluxes retains the design order of the original discrete operator for any diagonal norm SBP matrix $\mathcal{Q}$.

THEOREM 3.5. *A two-point entropy conservative flux can be extended to high order with formal boundary closures by using the form*

$$\bar{f}_i^{(S)} = \sum_{k=i+1}^{N} \sum_{\ell=1}^{i} 2 q_{(\ell,k)} \bar{f}_S\left(q_\ell, q_k\right), \quad 1 \le i \le N-1, \tag{3.13}$$

when the two-point nondissipative function from Tadmor [41] *is used:*

$$\bar{f}_S\left(q_k, q_\ell\right) = \int_0^1 g\left(w(q_k) + \xi\left(w(q_\ell) - w(q_k)\right)\right) \mathrm{d}\xi, \quad g(w(u)) = f(u). \tag{3.14}$$

The coefficient, $q_{(k,\ell)}$, corresponds to the (k,ℓ)th row and column in $\mathcal{Q}$, respectively.

Proof. To show the accuracy of approximation, the flux difference is expressed as

$$\bar{f}_i^{(S)} - \bar{f}_{i-1}^{(S)} = \sum_{k=i+1}^{N} \sum_{\ell=1}^{i} 2q_{(\ell,k)} \bar{f}_S\left(u_\ell, u_k\right) - \sum_{k=i}^{N} \sum_{\ell=1}^{i-1} 2q_{(\ell,k)} \bar{f}_S\left(u_\ell, u_k\right), \quad 2 \le i \le N-1,$$

which may be manipulated into the form (see [12, 13])

$$\bar{f}_i^{(S)} - \bar{f}_{i-1}^{(S)} = \sum_{j=1}^{N} 2q_{(i,j)} \bar{f}_S(u_i, u_j), \quad 1 \le i \le N. \tag{3.15}$$

This form facilitates an analysis by Taylor series at every solution point by using the expression for the two-point fluxes given in (3.14). The remainder of the proof is presented elsewhere [12, 13]. ∎

The final theorem establishes that the linear combination does indeed preserve the property of entropy conservation for any arbitrary diagonal norm SBP matrix $\mathcal{Q}$.

THEOREM 3.6. *A two-point high-order entropy conservative flux satisfying* (3.12) *with formal boundary closures can be constructed using* (3.13)*,*

$$\bar{f}_i^{(S)} = \sum_{k=i+1}^{N} \sum_{\ell=1}^{i} 2q_{(\ell,k)} \bar{f}_S\left(q_\ell, q_k\right), \quad 1 \le i \le N-1,$$

where $\bar{f}_S(q_\ell, q_k)$ is any two-point nondissipative function that satisfies the entropy conservation condition

$$\left(w_\ell - w_k\right)^T \bar{f}_S\left(q_\ell, q_k\right) = \psi_\ell - \psi_k. \tag{3.16}$$

The high-order entropy conservative flux satisfies an additional local entropy conservation property,

$$\mathbf{w}^T \mathcal{P}^{-1} \Delta \overline{\mathbf{f}}^{(S)} = \mathcal{P}^{-1} \Delta \overline{\mathbf{F}} = F_x(\mathbf{q}) + \mathcal{T}_d, \tag{3.17}$$

or, equivalently,

$$w_i^T \left(\bar{f}_i^{(S)} - \bar{f}_{i-1}^{(S)}\right) = \left(\bar{F}_i - \bar{F}_{i-1}\right), \quad 1 \le i \le N, \tag{3.18}$$

where

$$\bar{F}_i = \sum_{k=i+1}^{N} \sum_{\ell=1}^{i} q_{(\ell,k)} \left[\left(w_\ell + w_k\right)^T \bar{f}_S\left(q_\ell, q_k\right) - \left(\psi_\ell + \psi_k\right)\right], \quad 1 \le i \le N-1. \tag{3.19}$$

Proof. For brevity, the proof is not included herein but is reported elsewhere [12, 13]. ∎

Remark. The existence of a local second-order entropy flux satisfying the two-point shuffle relation given in (3.16) is a very strong constraint and has until recently been a computation bottleneck [24]. The two-point entropy consistent flux of Ismail and Roe [24] is used exclusively in this work and is discussed in section 6.1.2.

Remark. The entropy consistency proof is satisfied for all two-point fluxes that satisfy (3.16). The accuracy proof is proven only for fluxes in the integral form (3.14). Currently, the proof does not extend to any flux satisfying (3.16), so such fluxes should be validated for accuracy independent of Theorem 3.5.

3.2.3. Entropy stable viscous terms. Using the formalism introduced in section 2.1.2, viscous terms are derived that discretely mimic the continuous entropy properties. As with the continuous estimate, the proof requires the viscous fluxes to be written as functions of the discrete gradients of the entropy variables,

$$(\hat{c}_{11} w_x)_x = \mathcal{P}^{-1} \Delta \overline{\mathbf{f}}^{(v)} = \mathcal{D}_2(\hat{c}_{11})\mathbf{w} + \mathcal{T}_p, \qquad \mathcal{D}_2(\hat{c}_{11})\mathbf{w} = \mathcal{P}^{-1}\left(-\mathcal{D}^T \mathcal{P}[\hat{c}_{11}]\mathcal{D} + \mathcal{B}[\hat{c}_{11}]\mathcal{D}\right)\mathbf{w}. \tag{3.20}$$

The accuracy requirements are automatically satisfied. The coefficient matrix $[\hat{c}_{11}]$ is positive semidefinite because it is constructed from block-diagonal combinations of positive semidefinite matrices.

The contribution of the viscous terms to the semidiscrete entropy decay rate is

$$\mathbf{w}^T \Delta \overline{\mathbf{f}}^{(v)} = \mathbf{w}\mathcal{B}[\hat{c}_{11}]\mathcal{D}\mathbf{w} - (\mathcal{D}\mathbf{w})^T \mathcal{P}[\hat{c}_{11}](\mathcal{D}\mathbf{w}). \tag{3.21}$$

The last term is negative semidefinite. As with the continuous estimate given in (3.8), only the boundary term can produce a growth of the entropy, and thus the approximation of the viscous terms is entropy stable. (Well-posed boundary conditions that bound these terms are currently a topic of investigation.)

4. Entropy stable spectral collocation elements: Discontinuous interfaces. Entropy stable, conservative, and design order consistent interface operators are now presented. Inviscid and viscous coupling operators between adjoining elements can take many forms; a discontinuous penalty approach closely resembling that of a strong form nodal discontinuous Galerkin (DG) FEM method is adopted herein for both the inviscid and viscous terms.[2] Each is developed independently to guarantee an entropy stable inviscid penalty in the limit of vanishing viscosity.

The interface coupling of the inviscid terms is precisely equivalent to that used in the DG-FEM method. Two independent collocated solutions are defined on each side of an interface, and a single conservative interface flux is reconstructed from the collocated solutions. Herein, an interface flux that is more dissipative than an entropy conservative flux is used.

The coupling of the viscous terms is again reminiscent of the techniques used in the discontinuous Galerikin (DG) FEM method; the approach closely resembles the local DG (LDG) FEM method of Cockburn and Shu [10], although additional dissipation terms are added in the spirit of the internal penalty (IP) FEM approach of Wheeler [42] and Arnold [1].

The novelty of the current approach is that it uses entropy stable inviscid and viscous fluxes that preserve the accuracy and entropy estimate of the two adjoining elements. Thus, a global statement of accuracy and entropy stability for the Navier–Stokes equations is achieved. Note that any entropy stable inviscid flux would lead to a global entropy estimate, although the accuracy estimate would not necessarily be retained.

4.1. Navier–Stokes in one spatial dimension. Define an entropy *stable* inviscid interface flux $\mathbf{f}^{ssr}(q_i^{(-)}, q_i^{(+)})$ as the sum of an entropy *conservative* interface flux $\mathbf{f}^{sr}(q_i^{(-)}, q_i^{(+)})$ and a dissipation term $(\Lambda^I)[w_i^{(+)} - w_i^{(-)}]$:

$$\mathbf{f}^{ssr}(q_i^{(-)}, q_i^{(+)}) = \mathbf{f}^{sr}(q_i^{(-)}, q_i^{(+)}) + \Lambda^I [w_i^{(+)} - w_i^{(-)}], \tag{4.1}$$

[2]The combined interior/interface algorithm is essentially of the strong form nodal DG family, with collocated fluxes constructed to telescope the entropy across the element and the interface [21].

where Λ^I is a symmetric interface matrix with zero or negative eigenvalues. The entropy stable flux $\mathbf{f}^{ssr}(q_i^{(-)}, q_i^{(+)})$ is more dissipative than the entropy conservative inviscid flux given in (3.16), as is easily verified by contracting $\mathbf{f}^{ssr}(q_i^{(-)}, q_i^{(+)})$ against the entropy variables to yield the expression

$$(w_i^{(+)} - w_i^{(-)})^T \mathbf{f}^{ssr}(q_i^{(-)}, q_i^{(+)}) = \psi_i^{(+)} - \psi_i^{(-)} + (w_i^{(+)} - w_i^{(-)})^T \Lambda^I (w_i^{(+)} - w_i^{(-)}). \tag{4.2}$$

Next, consider two elements, each discretized with an entropy stable formulation described in the previous section. A coupling procedure between the adjoining elements that preserves the entropy stability of the inviscid and viscous terms in the Navier–Stokes equations can be constructed as follows:

$$\begin{aligned} \mathcal{P}_l[\tfrac{\partial q_l}{\partial t} + \Delta\overline{\mathbf{f}}_l - \mathcal{D}_l \hat{c}_{11} \mathbf{\Theta}_l] = \quad & [+\overline{\mathbf{f}}_i^{(-)} - \mathbf{f}^{ssr}(q_i^{(-)}, q_i^{(+)})] && \mathbf{e}_\mathbf{i}^{(-)} \\ + \quad & [-\tfrac{1}{2}(1+\alpha)(\hat{c}_{11}^{(-)}\Theta_i^{(-)} - \hat{c}_{11}^{(+)}\Theta_i^{(+)}) + \tfrac{1}{2}\Lambda^V(w_i^{(-)} - w_i^{(+)})] && \mathbf{e}_\mathbf{i}^{(-)}, \end{aligned} \tag{4.3a}$$

$$\mathcal{P}_l(\mathbf{\Theta}_l - \mathcal{D}_l w_l) = \quad [-\tfrac{1}{2}(1-\alpha)(w_i^{(-)} - w_i^{(+)})] \quad \mathbf{e}_\mathbf{i}^{(-)}, \tag{4.3b}$$

$$\begin{aligned} \mathcal{P}_r[\tfrac{\partial q_r}{\partial t} + \Delta\overline{\mathbf{f}}_r - \mathcal{D}_r \hat{c}_{11} \mathbf{\Theta}_r] = \quad & [-\overline{\mathbf{f}}_i^{(+)} + \mathbf{f}^{ssr}(q_i^{(-)}, q_i^{(+)})] && \mathbf{e}_\mathbf{i}^{(+)} \\ + \quad & [+\tfrac{1}{2}(1-\alpha)(\hat{c}_{11}^{(+)}\Theta_i^{(+)} - \hat{c}_{11}^{(-)}\Theta_i^{(-)}) + \tfrac{1}{2}\Lambda^V(w_i^{(+)} - w_i^{(-)})] && \mathbf{e}_\mathbf{i}^{(+)}, \end{aligned} \tag{4.3c}$$

$$\mathcal{P}_r(\mathbf{\Theta}_r - \mathcal{D}_r w_r) = \quad [+\tfrac{1}{2}(1+\alpha)(w_i^{(+)} - w_i^{(-)})] \quad \mathbf{e}_\mathbf{i}^{(+)}. \tag{4.3d}$$

The following nomenclature is used in (4.3). The subscripts l, r denote variables defined in the "left, right" elements, respectively. The first and third subequations describe the discretization of the conserved variables, q_l, q_r, while the second and fourth describe the discretization of the gradients of the entropy variables, $\mathbf{\Theta}_l, \mathbf{\Theta}_r$. The subscript i denotes an interface quantity, while the superscripts "$(-)$, $(+)$" denote the collocated values on the left and right sides of the interface, respectively. The vectors $\mathbf{e}_\mathbf{i}^{(-)}$ and $\mathbf{e}_\mathbf{i}^{(+)}$ are zero at all points except at the "$(-)$, $(+)$" interface points and enforce the penalties at the interface. The LDG penalty terms involve the coefficients $\frac{1}{2}(1 \pm \alpha)$, while the IP-FEM terms involve the parameter matrix Λ^V. The remainder of the penalty is the entropy stable inviscid contribution.

The entropy stability of (4.3) is established in the following theorem.

THEOREM 4.1. *The approximation of the one-dimensional Navier–Stokes equations given in* (4.3) *is entropy stable for any value of the parameter* α*, provided that the matrix* Λ^V *is negative semidefinite, i.e.,* $\Lambda^V \leq 0$.

Proof. Assume that suitable boundary conditions and initial data are provided and that an entropy stable formulation is used to discretize each adjoining element. Entropy stability of (4.3) follows immediately if the interface treatment at $x = x_i$ is more dissipative than an entropy conservative interface treatment.

The entropy method is used to prove the stability of (4.3). Multiplying the two discrete equations in the left element by w_l^T and $(\hat{c}_{11l}\,\mathbf{\Theta}_l)^T$, respectively, and the two discrete equations in the right element by w_r^T and $(\hat{c}_{11r}\,\mathbf{\Theta}_r)^T$, respectively, and then summing the four equations and collecting terms results in the expression

$$\tfrac{d}{dt}[\|S_l\|_{\mathcal{P}_l}^2 + \|S_r\|_{\mathcal{P}_r}^2] + 2[\,\|\sqrt{\hat{c}_{11l}}\,\mathbf{\Theta}_l\|_{\mathcal{P}_l}^2 + \|\sqrt{\hat{c}_{11r}}\,\mathbf{\Theta}_r\|_{\mathcal{P}_r}^2] = \Upsilon_i, \tag{4.4}$$

where

(4.5)
$$\begin{aligned}\Upsilon_i &= [w_l\hat{c}_{11l}\,\mathbf{\Theta}_l + \mathbf{\Theta}_l\hat{c}_{11l}\,w_l - F(q)]_{-1}^{i_-} + [w_r\hat{c}_{11r}\,\mathbf{\Theta}_r + \mathbf{\Theta}_r\hat{c}_{11r}\,w_r - F(q)]_{i_+}^{1}\\ &+ w_i^{(-)}(f(q_i^{(-)}) - \mathbf{f}^{ssr}(q_i^{(-)},q_i^{(+)})) - w_i^{(+)}(f(q_i^{(+)}) - \mathbf{f}^{ssr}(q_i^{(-)},q_i^{(+)}))\\ &+ w_i^{(-)}\,\Lambda^V[w_i^{(-)} - w_i^{(+)}] - (1+\alpha)\;w_i^{(-)}\,[\hat{c}_{11}^{(-)}\Theta_i^{(-)} - \hat{c}_{11}^{(+)}\Theta_i^{(+)}]\\ &- (1-\alpha)\;\Theta_i^{(-)}\,\hat{c}_{11}^{(-)}[w_i^{(-)} - w_i^{(+)}]\\ &+ w_i^{(+)}\,\Lambda^V[w_i^{(+)} - w_i^{(-)}] + (1-\alpha)\;w_i^{(+)}\,[\hat{c}_{11}^{(+)}\Theta_i^{(+)} - \hat{c}_{11}^{(-)}\Theta_i^{(-)}]\\ &+ (1+\alpha)\;\Theta_i^{(+)}\,\hat{c}_{11}^{(+)}[w_i^{(+)} - w_i^{(-)}].\end{aligned}$$

The viscous dissipation terms $\|\sqrt{\hat{c}_{11l}}\,\mathbf{\Theta}_l\|^2_{\mathcal{P}_l}$ and $\|\sqrt{\hat{c}_{11r}}\,\mathbf{\Theta}_r\|^2_{\mathcal{P}_r}$ are uniformly dissipative. Thus, entropy stability of (4.4) follows immediately if the term Υ_i is dissipative. Note that Υ_i is composed of both inviscid and viscous terms; i.e., $\Upsilon_i = \Upsilon_i^I + \Upsilon_i^V$. The inviscid and viscous terms are bounded individually to guarantee that the inviscid terms are stable in the limit of $Re \to \infty$.

Inviscid stability. The inviscid interface terms in Υ_i are

(4.6)
$$\begin{aligned}\Upsilon_i^I &= F(q_i^{(+)}) - F(q_i^{(-)})\\ &+ w_i^{(-)}(f(q_i^{(-)}) - \mathbf{f}^{ssr}(q_i^{(-)},q_i^{(+)})) - w_i^{(+)}(f(q_i^{(+)}) - \mathbf{f}^{ssr}(q_i^{(-)},q_i^{(+)})).\end{aligned}$$

Substituting the definitions for the entropy fluxes,

$$F(q_i^{(+)}) = w_i^{(+)}f(q_i^{(+)}) - \psi_i^{(+)} \quad ; \quad F(q_i^{(-)}) = w_i^{(-)}f(q_i^{(-)}) - \psi_i^{(-)}\,,$$

into (4.6) and simplifying using (4.2) yields the equation

(4.7)
$$\Upsilon_i^I = \left(w_i^{(+)} - w_i^{(-)}\right)^T \mathbf{f}^{ssr}(q_i^{(-)},q_i^{(+)}) - (\psi_i^{(+)} - \psi_i^{(-)}) = (w_i^{(+)} - w_i^{(-)})^T\Lambda^I(w_i^{(+)} - w_i^{(-)}),$$

which is a dissipative term provided Λ^I is negative semidefinite.

Viscous stability. The viscous interface term in Υ_i is

(4.8)
$$\begin{aligned}\Upsilon_i^V &= [w_l\hat{c}_{11l}\,\mathbf{\Theta}_l + \mathbf{\Theta}_l\hat{c}_{11l}\,w_l]_{-1}^{i_-} + [w_r\hat{c}_{11r}\,\mathbf{\Theta}_r + \mathbf{\Theta}_r\hat{c}_{11r}\,w_r]_{i_+}^{1}\\ &+ w_i^{(-)}\,\Lambda^V[w_i^{(-)} - w_i^{(+)}] - (1+\alpha)\;w_i^{(-)}\,[\hat{c}_{11}^{(-)}\Theta_i^{(-)} - \hat{c}_{11}^{(+)}\Theta_i^{(+)}]\\ &- (1-\alpha)\;\Theta_i^{(-)}\,\hat{c}_{11}^{(-)}[w_i^{(-)} - w_i^{(+)}]\\ &+ w_i^{(+)}\,\Lambda^V[w_i^{(+)} - w_i^{(-)}] + (1-\alpha)\;w_i^{(+)}\,[\hat{c}_{11}^{(+)}\Theta_i^{(+)} - \hat{c}_{11}^{(-)}\Theta_i^{(-)}]\\ &+ (1+\alpha)\;\Theta_i^{(+)}\,\hat{c}_{11}^{(+)}[w_i^{(+)} - w_i^{(-)}],\end{aligned}$$

which simplifies to

$$\Upsilon_i^V = [w_i^{(-)} - w_i^{(+)}]\Lambda^V[w_i^{(-)} - w_i^{(+)}], \tag{4.9}$$

and is dissipative provided Λ^V is negative semidefinite. Combining (4.7) and (4.9) yields the desired result

$$\Upsilon_i = \Upsilon_i^I + \Upsilon_i^V = [w_i^{(-)} - w_i^{(+)}](\Lambda^I + \Lambda^V)[w_i^{(-)} - w_i^{(+)}]. \qquad \square$$

Remark. The parameter values $\alpha = 0$ and $\alpha = \pm 1$ yield a symmetric LDG and "flip-flop" narrow stencil LDG penalty, respectively. An LDG value of $\alpha = 0$ produces a global discrete operator that has a neutrally damped spurious eigenmode. The IP dissipation effectively damps this mode.

Remark. The first component of the vector $(\hat{c}_{11l}\,\mathbf{\Theta}_l)^T$ is zero, as are the first row and column of the matrix $(\hat{c}_{11l})$. Thus, the matrix $(\hat{c}_{11l})$ and $\sqrt{\hat{c}_{11l}}$ are only semidefinite. The proof is still valid because definiteness is never assumed.

Remark. Extension of Theorem 4.1 to three dimensions follows immediately. Contract the two conservative equations with the entropy variables and the six LDG gradient equations with their respective viscous flux $\overline{\mathbf{f}}^{(v)}$ on either side of the interface.

4.1.1. Inviscid interface dissipation. The entropy stable interface flux $\mathbf{f}^{ssr}(q_i^{(-)}, q_i^{(+)})$ used in (4.2) is composed of the sum of an entropy conservative flux $\mathbf{f}^{sr}(q_i^{(-)}, q_i^{(+)})$ and a dissipation term $(\Lambda^I)[w_i^{(-)} - w_i^{(+)}]$. Adjusting the inviscid dissipation matrix (Λ^I) leads to different levels of interface damping. (See (4.7) for the precise relationship between Λ^I and entropy dissipation.)

A local Lax–Friedrichs interface flux is typically defined as

$$\begin{array}{rcl} \mathbf{f}^{llf}(q_i^{(-)}, q_i^{(+)}) & = & \frac{1}{2}(\mathbf{f}(q_i^{(-)}) + \mathbf{f}(q_i^{(+)})) \; - \; 1/2\mathcal{Y}|\lambda_{max}^{llf}|\mathcal{Y}^T(w_i^{(-)} - w_i^{(+)}), \\ \lambda_{max}^{llf} & = & \max_{[(-),(+)]} |\mathbf{f}'(q)|, \end{array} \tag{4.10}$$

where $|\mathbf{f}'(q)|$ denotes the maximum eigenvalue of $\frac{\partial f}{\partial q}$. Note that scaling the dissipation coefficient λ_{max}^{llf} by any positive factor greater than one produces more dissipation (e.g., the global maximum value rather than the local value).

The maximum eigenvalue λ_{max}^{llf} is well approximated in the context of the Euler equations of gas dynamics by the expression

$$\lambda_{max} = \left[\frac{1}{2}((u^{(-)})^4 + (c^{(-)})^4 + (u^{(+)})^4 + (c^{(+)})^4)\right]^{\frac{1}{4}} \; \geq \; \lambda_{max}^{llf}. \tag{4.11}$$

Define an *entropy stable local Lax–Friedrichs* flux by the expression

$$\mathbf{f}^{ssllf}(q_i^{(-)}, q_i^{(+)}) \; = \; \mathbf{f}^{sr}(q_i^{(-)}, q_i^{(+)}) \; + \; 1/2\mathcal{Y}|\lambda_{max}^{llf}|\mathcal{Y}^T(w_i^{(-)} - w_i^{(+)}) \, . \tag{4.12}$$

Note that (4.12) differs from (4.10); the linear average interface flux $\frac{1}{2}(f(q_i^{(-)}) + f(q_i^{(+)}))$ in $\mathbf{f}^{llf}(q_i^{(-)}, q_i^{(+)})$ is replaced with the nonlinear average entropy conservative flux $\mathbf{f}^{sr}(q_i^{(-)}, q_i^{(+)})$. By definition, the flux $\mathbf{f}^{ssllf}(q_i^{(-)}, q_i^{(+)})$ is entropy stable as given in (4.1).

Both forms of Lax–Friedrichs dissipation are overly dissipative for convective waves at the interface. A more refined approach dissipates each characteristic wave based on the magnitude of its eigenvalue. A flux that includes dissipation of this form is denoted an *entropy stable characteristic* flux and is implemented as

$$\begin{array}{c} \mathbf{f}^{ssc}(q_i^{(-)}, q_i^{(+)}) \; = \; \mathbf{f}^{sr}(q_i^{(-)}, q_i^{(+)}) \; + \; 1/2\mathcal{Y}|\lambda|\mathcal{Y}^T(w_i^{(-)} - w_i^{(+)}) \, , \\ \mathbf{f}'(q) \; = \; \mathcal{Y}\lambda\mathcal{Y}^T \quad ; \quad \frac{\partial q}{\partial w} \; = \; \mathcal{Y}\mathcal{Y}^T. \end{array} \tag{4.13}$$

Note that the relation $q_w = \mathcal{Y}\mathcal{Y}^T$ is achieved by an appropriate scaling of the rotation eigenvectors. See the work of Merriam [32] for more details. Unless otherwise noted, the entropy stable characteristic flux is used in all test simulations.

5. The comparison approach using entropy conservative schemes. Entropy conservative formulations suffer breakdown when used without dissipation to capture shocks. The entropy discontinuity at the shock is inconsistent with the underlying premise of an isentropic algorithm, and large amplitude oscillations around the shock are the result. More problematic, however, is that entropy conservative formulations cannot converge to the weak solution; there is no mechanism to admit the dissipation physically required at the shock.

Herein a comparison approach is adopted to facilitate the addition of dissipation to the entropy conservative baseline formulation. A comparison approach uses a companion algorithm in conjunction with an entropy conservative formulation. At every point, the entropy generated by the companion scheme is compared with that of the entropy datum. If the entropy condition is violated (i.e., the inequality derived in (3.9)), then more dissipation is added locally. Local conditions that guarantee the entropy stability of a comparison approach are now derived.

An inviscid semidiscrete condition analogous to (3.11) that guarantees entropy stability is

$$\mathbf{w}^T \mathcal{P} \mathbf{q}_t + F(q_N) - F(q_1) \leq \mathbf{w}^T (\mathbf{g}_b + \mathbf{g}_i), \tag{5.1}$$

which is satisfied if the "baseline" entropy stable inviscid fluxes satisfy the comparison condition

$$\mathbf{w}^T \Delta \overline{\mathbf{f}} \geq \mathbf{1}^T \Delta \overline{\mathbf{F}}. \tag{5.2}$$

Using the result for the entropy conservative flux in (3.11), this condition can be rewritten as

$$\mathbf{w}^T \Delta \overline{\mathbf{f}} \geq \mathbf{w}^T \Delta \overline{\mathbf{f}}^{(S)}.$$

Substituting the generalized SBP property,[3]

$$\mathbf{w}^T (\tilde{\mathcal{B}} - \tilde{\Delta})(\overline{\mathbf{f}}^{(S)} - \overline{\mathbf{f}}) = \mathbf{w}^T \tilde{\Delta}(\overline{\mathbf{f}} - \overline{\mathbf{f}}^{(S)}) = \mathbf{w}^T \tilde{\Delta}([\overline{\mathbf{f}}] - [\overline{\mathbf{f}}^{(S)}])\bar{\mathbf{1}} \leq 0, \tag{5.3}$$

yields the sufficient local conditions for entropy stability,

$$\mathbf{w}^T \tilde{\Delta}[\overline{\mathbf{f}}] \leq \mathbf{w}^T \tilde{\Delta}[\overline{\mathbf{f}}^{(S)}], \tag{5.4}$$

or, in indicial form,

$$(w_{i+1} - w_i)^T (\bar{f}_i - \bar{f}_i^{(S)}) \leq 0, \quad i = 1, 2, \ldots, N-1. \tag{5.5}$$

These conditions can be enforced by using a limiter function of the form

$$\bar{f}_i^{(SS)} = \bar{f}_i + \delta(\bar{f}_i^{(S)} - \bar{f}_i), \; \delta = \frac{\sqrt{b^2 + c^2} - b}{\sqrt{b^2 + c^2}}, \; b = (w_{i+1} - w_i)^T (\bar{f}_i^{(S)} - \bar{f}_i), \; c = 10^{-12}, \tag{5.6}$$

with $\bar{f}_i^{(SS)}$ the entropy stabilized flux. The pointwise entropy stability conditions given in (5.5) and (5.6) are valid for any pair of comparison fluxes $\bar{f}_i$ and $\bar{f}_i^{(S)}$ provided that both can be expressed in telescopic flux form. Note, however, that the local conditions in (5.5) do not provide insight on the magnitude of dissipation required to achieve a nonoscillatory shock.

5.1. Candidate schemes for a comparison approach. Both the entropy conservative and companion operators should (ideally) be of equivalent order; the formal order of the comparison approach is the lesser of the two individual orders. A natural high-order comparison candidate for shocks is a WENO operator of comparable accuracy. This is the strategy adopted in [13]. WENO schemes are design

[3]The bracket nomenclature around a vector denotes a diagonal matrix with vector elements injected on the diagonal.

order accurate for smooth solutions and capture shocks with minimal oscillations but can be overly dissipative for underresolved smooth features and are computationally intensive. Furthermore, they are difficult to formulate in the context of unstructured FEMs, owing to the extensive set of smooth interpolants that are needed, some of which belong to adjoining elements.

A second approach is to use a "troubled element" detector to identify elements that contain discontinuities. This information is then used to switch from the baseline high-order formulation to a shock capturing approach. One could use a conventional shock capturing approach (e.g., monotonic upstream-centered scheme for conservation laws (MUSCL), TVD, piecewise parabolic method (PPM), total variation bounded (TVB)) in the troubled elements, keeping in mind that the formal accuracy drops locally to first order. Provided that the smoothness detector is sufficiently discriminating between shocks and smooth extrema, the drop in local accuracy does not further degrade the formal accuracy since captured shocks are inevitably first-order.

5.2. Entropy stable spectral collocation element: Dissipation. Four forms of dissipation appear in SSSCE schemes used to simulate the Navier–Stokes equations. The physical viscous terms and dissipative Dirichlet or Neumann boundary conditions appear naturally in the equations. A third dissipation arises at element interfaces—the result of upwinding the interface fluxes. The first three dissipative mechanisms generally are not sufficient to stabilize the algorithm for capturing strong discontinuities. Finally, a fourth dissipation is introduced locally during the entropy correction phase of the algorithm, but only where the entropy condition is violated. The level of dissipation depends on the dissipative properties of the companion operator.

The goal herein is to demonstrate the potential of the comparison approach used in conjunction with the entropy conservative spectral collocation element operator. Three elementary companion operators are constructed and used with the baseline entropy conservative element operator. The first is a P3 WENO element scheme. The basic algorithm is constructed following the ideas provided in [44]. Only the inter-element stencil biasing mechanics is included in the formulation. (Indeed, obtaining smooth interpolants from adjoining elements is nontrivial and is the topic of a future paper.)

A second approach uses a piecewise linear MUSCL reconstruction companion operator. In this case, the MUSCL reconstruction is implemented using the data on the LGL grid and intermediate fluxes. Local data as well as that from the two adjoining elements are used in the reconstruction. The limiter function of Koren [27] is used in this study.

The final companion operator is the strong form nodal DG spectral collocation scheme, recast into flux conservation form. This operator does not introduce dissipation within the element and uses the same interface fluxes. Indeed, the additional dissipation arises solely from the differences between two internally nondissipative operators. The entropy stabilization arising from this operator is design order small for smooth solutions. At shocks, however, the two fluxes differ significantly owing to different nonlinear aliasing properties of the internal fluxes. Furthermore, the DG does not have a stability proof and can be unstable at shocks.

The studies that follow differentiate the different forms of dissipation. Although the optimal companion operator for the SSSCE schemes remains to be determined, it is demonstrated herein that very little dissipation is required for the companion operator. The natural and interface dissipation combined with the entropy correction procedure is shown to be sufficient to stabilize the capturing of strong shocks.

6. Entropy analysis for the Navier–Stokes equations.

6.1. Euler and Navier–Stokes equations. The calorically perfect form of the Navier–Stokes equations is given in (2.1). The conservative variables for the Navier–Stokes equations are

$$q = (\rho, \rho\upsilon_1, \rho\upsilon_2, \rho\upsilon_3, \rho E)^T, \tag{6.1}$$

where ρ denotes density, $\upsilon = (\upsilon_1, \upsilon_2, \upsilon_3)^T$ is the velocity vector, and E is the specific total energy. The convective fluxes are

$$f^i = (\rho\upsilon_i, \rho\upsilon_i\upsilon_1 + \delta_{i1}p, \rho\upsilon_i\upsilon_2 + \delta_{i2}p, \rho\upsilon_i\upsilon_3 + \delta_{i3}p, \rho\upsilon_i H)^T, \tag{6.2}$$

where p represents pressure, $H = E + p/\rho$ is the specific total enthalpy, and δ_{ij} is the Kronecker delta. The viscous flux terms are

$$f^{(v)i} = (0, \tau_{i1}, \tau_{i2}, \tau_{i3}, \tau_{ji}\upsilon_j - \mathsf{q}_i)^T, \tag{6.3}$$

where the shear stress and heat flux are

$$\tau_{ij} = \mu\left((\upsilon_i)_{x_j} + (\upsilon_j)_{x_i} - \delta_{ij}\frac{2}{3}(\upsilon_\ell)_{x_\ell}\right) \quad ; \quad \mathsf{q}_i = -\kappa T_{x_i}. \tag{6.4}$$

The variable T denotes the static temperature, with $\mu = \mu(T)$ and $\kappa = \kappa(T)$ the dynamic viscosity and thermal conductivity, respectively.

The constitutive relations for a perfect gas are

$$h = H - \frac{1}{2}\upsilon_j\upsilon_j = c_pT \quad ; \quad p = \rho RT \quad ; \quad R = \frac{R_u}{MW} \quad ; \quad c = \sqrt{\gamma RT} \quad ; \quad \gamma = \frac{c_p}{c_p - R}, \tag{6.5}$$

where c_p is the constant specific heat, R_u is the universal gas constant, MW is the molecular weight of the gas, and c is the speed of sound. In the entropy analysis that follows, the definition of the thermodynamic entropy is the explicit form

$$s = \frac{R}{\gamma - 1}\log\left(\frac{T}{T_0}\right) - R\log\left(\frac{\rho}{\rho_0}\right), \tag{6.6}$$

where T_0 and ρ_0 are the reference temperature and density, respectively.

6.1.1. Entropy analysis. A continuous entropy stability analysis is conducted first to illustrate the entropy characteristics of the governing equations. Discrete spatial operators that mimic these continuous properties are derived next via semidiscrete entropy analysis.

The entropy–entropy flux pair and the potential–potential flux pair for the Navier–Stokes equations are

$$S = -\rho s, \quad F^i = -\rho\upsilon_i s \quad ; \quad \varphi = \rho R, \quad \psi^i = \rho\upsilon_i R. \tag{6.7}$$

The entropy variables consistent with the definitions provided in (6.7) are

$$w = S_q^T = \left(\frac{h}{T} - s - \frac{\upsilon_j\upsilon_j}{2T}, \frac{\upsilon_1}{T}, \frac{\upsilon_2}{T}, \frac{\upsilon_3}{T}, -\frac{1}{T}\right)^T \tag{6.8}$$

and may be shown to have a one-to-one mapping with the conservative variables provided $\rho, T > 0$. Expressly,

$$\zeta^T S_{qq}\zeta^T > 0 \quad \forall\zeta \neq 0, \quad \rho, T > 0.$$

The entropy equation is constructed by contracting the Navier–Stokes equations with the entropy variables. The differential and integral forms of the entropy equation are given by (3.7) and (3.8).

6.1.2. Entropy stable spatial discretization. The inviscid terms in the discretization of the Navier–Stokes equations are calculated using (3.13); the two-point entropy conservative flux is that of Ismail and Roe [24]. Although this flux is complicated, it is the first entropy conservative flux for the convective terms with low enough computational cost to be implemented in a practical simulation code. Previously, Tadmor [40] derived an entropy conservative flux form that required integration through phase space, but this was deemed too expensive to be practical.

7. Accuracy validation.

7.1. Test equations. The accuracy and robustness of the algorithms developed herein are tested using four smooth and three discontinuous problems. The smooth problems are the nonlinear Burgers equation, the propagation of an isentropic compressible Euler vortex, and the propagation of the viscous Navier–Stokes shock without and with an entropy correction. All smooth problems demonstrate the design order convergence of the new entropy conservative formulation. All the discontinuous problems involve simulations using the one-dimensional Euler equations and include the Riemann shock tube of Sod, a sine-shock interaction test case, and a simulation of colliding blast waves.

7.1.1. The Burgers equation. The nonlinear Burgers equation is a one-dimensional model for the inviscid-viscous interaction found in the full Navier–Stokes equation. The Burgers equation is given by

$$\begin{array}{c} \frac{\partial u}{\partial t} \,+\, \frac{1}{2}\frac{\partial u^2}{\partial x} \,=\, \epsilon\frac{\partial^2 u}{\partial x^2} \quad ; \quad -1 \le x \le 1\,;\; t >= 0, \\ \alpha u(-1,t) - \epsilon u_x(-1,t) = g_{-1}(t)\,,\; \beta u(-1,t) + \epsilon u_x(-1,t) = g_{-1}(t)\,. \end{array} \tag{7.1}$$

An exact solution is given by

$$u(x,t) \,=\, \frac{a\exp((b-a)(x-ct-d)/(2\epsilon)+b}{1\exp((b-a)(x-ct-d)/(2\epsilon)+1} \quad ; \quad a=-\tfrac{1}{2}, b=1, c=\tfrac{1}{2}(a+b), d=\tfrac{1}{2}. \tag{7.2}$$

Initial and boundary data consistent with the exact solution are provided.

7.1.2. Isentropic vortex. The isentropic vortex is an exact solution to the Euler equations and is an excellent test of the accuracy and functionality of the inviscid components of a Navier–Stokes solver. It is fully described by

$$\begin{array}{rcl} f(x,y,z,t) &=& 1 - \Big[(x - x_0 - U_\infty\cos(\alpha)\,t)^2 + (y - y_0 - U_\infty\sin(\alpha)\,t)^2\Big], \\ T(x,y,z,t) &=& \big[1 - \epsilon_v^2 M_\infty^2 \frac{\gamma-1}{8\pi^2}\exp\left(f(x,y,z,t)\right)\big], \quad \rho(x,y,z,t) \,=\, T^{\frac{1}{\gamma-1}}, \\ u(x,y,z,t) &=& U_\infty\cos(\alpha) - \epsilon_v\frac{y-y_0-U_\infty\sin(\alpha)t}{2\pi}\exp\big(\frac{f(x,y,z,t)}{2}\big), \\ v(x,y,z,t) &=& U_\infty\sin(\alpha) - \epsilon_v\frac{x-x_0-U_\infty\cos(\alpha)t}{2\pi}\exp\big(\frac{f(x,y,z,t)}{2}\big), \\ w(x,y,z,t) &=& 0. \end{array} \tag{7.3}$$

In this study the values $U_\infty \,=\, M_\infty c_\infty$, $\epsilon_v = 5.0$, $M_\infty = 0.5$, and $\gamma = 1.4$ are used.

The Cartesian grid test case is described by

$$x \in (-15,15), \quad y \in (-15,15), \quad (x_0,y_0) \,=\, (0,0), \quad \alpha = 0.0, \quad t \ge 0.$$

7.1.3. The viscous shock. The Navier–Stokes equations support an exact solution for the viscous shock profile, under the assumption that the Prandtl number is $Pr \,=\, \frac{3}{4}$. Mass and total enthalpy are constant across a shock. Furthermore, if

$Pr = \frac{3}{4}$, then the momentum and energy equations are redundant. The single momentum equation across the shock is given by

$$\begin{gathered} \alpha v v_x - (v-1)(v-v_f) = 0 \quad ; \quad -\infty \le x \le \infty \quad , \quad t \ge 0; \\ v \;=\; \tfrac{u}{u_L} \;;\; v_f = \tfrac{u_R}{u_L} \;;\; \alpha \;=\; \tfrac{\gamma-1}{2\gamma}\tfrac{\mu}{Pr\,m}. \end{gathered} \tag{7.4}$$

An exact solution is obtained by solving the momentum equation for the velocity profile:

$$x \;=\; \tfrac{1}{2}\alpha\left(\mathrm{Log}|(v-1)(v-v_f)| + \tfrac{1+v_f}{1-v_f}\mathrm{Log}|\tfrac{v-1}{v-v_f}|\right). \tag{7.5}$$

A moving shock is recovered by applying a uniform translation to the solution. A full derivation of this solution appears in the thesis of Fisher [11].

7.1.4. Sod's shock tube. Sod's shock tube problem is a classical Riemann problem that evaluates the behavior of a numerical method when a shock, expansion, and contact discontinuity are present. Of particular interest is smearing in the shock and contact, or oscillations, at any of the discontinuities. Sod's problem is initialized with

$$\begin{gathered} \rho(x) = \begin{cases} 1, & x < 0.5, \\ 1/8, & x \ge 0.5, \end{cases} \qquad p(x) = \begin{cases} 1, & x < 0.5, \\ 1/10, & x \ge 0.5, \end{cases} \\ u(x) = 0, \qquad x \in (0,1), \quad t \ge 0. \end{gathered} \tag{7.6}$$

All simulations use the value $\gamma = 7/5$ for the ratio of specific heats.

7.1.5. Sine-shock interaction. Numerical results are presented for the shock entropy-wave interaction problem. The solution of this benchmark problem contains both strong discontinuities and smooth structures and is well suited for testing high-order shock capturing schemes. The governing equations are the time-dependent one-dimensional Euler equations subject to the following initial conditions:

$$(\rho, u, p) = \begin{cases} (3.857134, 2.629369, 10.33333) & \text{if} \quad 0 \le x < 4.5, \\ (1 + 0.2\sin 5x, 0, 1) & \text{if} \quad 4.5 \le x \le 9. \end{cases} \tag{7.7}$$

The governing equations are integrated in time up to $t = 1.8$. The exact solution to this problem is not available. Therefore, a numerical solution that is obtained using 1024 uniformly distributed $P3$ elements is used as the reference solution.

7.1.6. Blast wave. The final problem provides a severe test of the robustness of the entropy stabilized algorithm by simulating the collision of two strong shock waves. It is motivated by the test case originally proposed by Woodward and Colella [43]. The governing equations are the time-dependent one-dimensional Euler equations subject to the following initial conditions:

$$(\rho, u, p) = \begin{cases} \left(1, 0, 10^{+3}\right) & \text{if} \quad 0 \le x < 1.7, \\ \left(1, 0, 10^{-2}\right) & \text{if} \quad 1.7 \le x < 2.5, \\ \left(1, 0, 10^{+2}\right) & \text{if} \quad 2.5 \le x < 3.4. \end{cases} \tag{7.8}$$

The governing equations are integrated in time to $t = 0.038$. The exact solution to this problem is not available. A reference numerical solution is obtained using 1024 uniformly distributed $P3$ elements. Coarse grids and high polynomial orders ($P \le 9$) are used in the simulations to test the likelihood of algorithmic failure due to negative pressures.

7.2. Test results. Smooth and discontinuous sets of problems are simulated. All smooth tests include elements of polynomial degrees $1 \leq p \leq 4$. Three smooth tests are performed without an entropy correction (Tables 1, 2, and 3), and one is performed with an entropy correction (Table 4). All tests include a uniform grid refinement study performed using a grid-doubling procedure. When possible, a randomly distributed grid is used. A properly nested set of uniformly refined random grids is generated as follows. First, a random grid is generated at the coarsest resolution. This grid is then scaled and replicated 2^s, $3 \leq s \leq 8$, times on the intervals $-1 \leq x, y \leq 1$. Thus, the randomness of the coarsest grid is preserved on all levels. Polynomial degrees $1 \leq p \leq 9$ are used for the discontinuous problems. The unusually high polynomial degrees are used to assess the robustness of dissipation strategies. All simulations are advanced in time using a fourth-order low-storage Runge–Kutta scheme [7]. A suitably small time step is chosen to ensure that temporal error is subordinate to spatial error and does not contaminate the results obtained in the spatial accuracy studies.

7.3. Smooth tests.

7.3.1. The nonlinear Burgers equation. Elsewhere [3], design order convergence of $p + 1$ in both the L^2- and L^∞-norms is demonstrated on the linear wave equation. The first test presented herein extends these results to include nonlinear hyperbolic and parabolic terms. Table 1 contains data from both a uniform and nonuniform grid refinement study of the nonlinear Burgers equation. The nonuniform grid refinement study is included to identify superconvergence resulting from fortuitous cancellation of viscous error terms at element interfaces. (See [9] for a discussion of this phenomenon.)

Sharp design order convergence of $p+1$ is achieved in both the L^2- and L^∞-norms on the uniform grid for polynomials of even order. This sharp convergence may be the result of fortuitous cancellation of errors. Design order convergence is achieved asymptotically for polynomials of odd order in both L^2 and L^∞. The nonuniform refinement study shows asymptotic design order convergence for both even and odd polynomial orders.

This test verifies that the superconvergence observed in the linear advection study extends to nonlinear inviscid terms and that the entropy stable LDG implementation is design order accurate for the viscous terms. Furthermore, superconvergence may be achieved on irregular grids.

7.3.2. The Euler vortex. The convergence rate for the isentropic Euler vortex is evaluated on a properly nested sequence of uniform two-dimensional grids. The vortex profile is initially located in the middle of the domain and is simulated until $t = 0.25$. The reference Mach number is $M = 0.5$, and the translation velocity of the vortex is unity. The errors for the uniform grids are shown in Table 2.

TABLE 1
Error convergence is shown for the nonlinear Burgers equation.

	Uniform grid				Nonuniform grid			
$p = 01$	L^2 error	L^2 rate	L^∞ error	L^∞ rate	L^2 error	L^2 rate	L^∞ error	L^∞ rate
8	1.16E-02		2.40E-02		1.77E-02		2.94E-02	
16	4.43E-03	-1.38	9.67E-03	-1.31	5.65E-03	-1.64	1.25E-02	-1.24
32	1.55E-03	-1.51	3.56E-03	-1.44	1.87E-03	-1.59	4.36E-03	-1.51
64	4.94E-04	-1.65	1.19E-03	-1.57	5.66E-04	-1.72	1.41E-03	-1.62
128	1.46E-04	-1.75	3.74E-04	-1.67	1.66E-04	-1.76	4.56E-04	-1.62
256	4.13E-05	-1.82	1.13E-04	-1.73	4.69E-05	-1.82	1.35E-04	-1.75
512	1.13E-05	-1.86	3.29E-05	-1.77	1.29E-05	-1.86	3.99E-05	-1.76
1024	3.04E-06	-1.89	9.36E-06	-1.81	3.44E-06	-1.90	1.12E-05	-1.82
$p = 02$								
8	1.00E-03		2.42E-03		2.04E-03		3.91E-03	
16	1.14E-04	-3.13	3.08E-04	-2.97	2.20E-04	-3.21	5.25E-04	-2.89
32	1.42E-05	-3.01	3.83E-05	-3.00	4.23E-05	-2.37	1.16E-04	-2.17
64	1.78E-06	-2.99	4.75E-06	-3.00	6.54E-06	-2.69	1.82E-05	-2.67
128	2.23E-07	-2.99	5.94E-07	-2.99	1.00E-06	-2.70	3.02E-06	-2.58
256	2.79E-08	-2.99	7.44E-08	-2.99	1.50E-07	-2.73	4.89E-07	-2.62
512	3.49E-09	-2.99	9.31E-09	-2.99	2.19E-08	-2.78	7.61E-08	-2.68
1024	4.36E-10	-2.99	1.16E-09	-2.99	3.07E-09	-2.83	1.14E-08	-2.73
$p = 03$								
8	7.83E-05		2.01E-04		2.23E-04		5.16E-04	
16	7.87E-06	-3.31	2.41E-05	-3.05	2.26E-05	-3.30	5.69E-05	-3.18
32	7.55E-07	-3.38	2.30E-06	-3.38	1.49E-06	-3.92	4.47E-06	-3.66
64	6.79E-08	-3.47	2.09E-07	-3.46	1.26E-07	-3.56	4.02E-07	-3.47
128	5.68E-09	-3.57	1.76E-08	-3.57	1.04E-08	-3.59	3.30E-08	-3.60
256	4.43E-10	-3.67	1.38E-09	-3.66	8.05E-10	-3.68	2.62E-09	-3.65
512	3.26E-11	-3.76	1.02E-10	-3.75	5.91E-11	-3.76	1.95E-10	-3.74
1024	2.31E-12	-3.81	7.59E-12	-3.75	4.14E-12	-3.83	1.38E-11	-3.81
$p = 04$								
8	5.51E-06		1.28E-05		1.26E-05		3.53E-05	
16	1.22E-07	-5.49	4.57E-07	-4.80	4.72E-07	-4.74	1.67E-06	-4.39
32	3.60E-09	-5.08	1.32E-08	-5.11	3.39E-08	-3.79	1.20E-07	-3.80
64	1.11E-10	-5.01	4.13E-10	-5.00	1.66E-09	-4.35	5.83E-09	-4.36
128	3.66E-12	-4.92	1.37E-11	-4.91	7.69E-11	-4.42	2.87E-10	-4.34
256	2.83E-13	-3.69	1.67E-12	-3.03	3.38E-12	-4.50	1.32E-11	-4.44
512	3.08E-14	-3.20	1.19E-13	-3.81	1.41E-13	-4.58	6.00E-13	-4.45
1024	3.65E-14	0.24	7.21E-14	-0.71	3.67E-14	-1.94	7.79E-14	-2.94

TABLE 2
Error convergence is shown for the isentropic Euler vortex equation.

Nested 2D nonuniform grids							
Grid	L^2 error	L^2 rate	L^∞ error	L^∞ rate	SSDC cost	NDG cost	Overhead
$p = 01$							
008x008	2.46E-03		1.04E-02		1	1	1.25
016x016	8.74E-04	-1.49	4.52E-03	-1.20	3	2	1.24
032x032	2.86E-04	-1.61	1.78E-03	-1.34	4	4	1.23
064x064	7.98E-05	-1.84	5.63E-04	-1.65	29	22	1.32
128x128	2.07E-05	-1.94	1.45E-04	-1.95	179	150	1.19
256x256	5.43E-06	-1.92	3.80E-05	-1.93	1348	1113	1.21
$p = 02$							
008x008	7.20E-05		4.55E-04		1	1	1.40
016x016	1.24E-05	-2.54	9.53E-05	-2.25	4	2	1.41
032x032	1.75E-06	-2.82	1.95E-05	-2.28	14	10	1.34
064x064	2.24E-07	-2.96	2.64E-06	-2.88	118	87	1.36
128x128	3.00E-08	-2.89	3.20E-07	-3.04	641	481	1.33
256x256	4.18E-09	-2.84	4.79E-08	-2.74	3570	2632	1.35
$p = 03$							
008x008	2.39E-06		2.27E-05		2	1	1.60
016x016	1.72E-07	-3.79	2.12E-06	-3.42	12	7	1.65
032x032	1.12E-08	-3.93	1.72E-07	-3.62	46	30	1.53
064x064	7.09E-10	-3.98	1.04E-08	-4.03	249	167	1.48
128x128	4.59E-11	-3.94	6.90E-10	-3.92	1391	974	1.42
$p = 04$							
008x008	3.37E-08		3.33E-07		8	4	1.81
016x016	1.68E-09	-4.32	2.21E-08	-3.91	32	18	1.77
032x032	5.14E-11	-5.03	7.26E-10	-4.93	84	53	1.56
064x064	1.65E-12	-4.95	2.18E-11	-5.05	463	286	1.61
128x128	7.48E-13	-1.14	4.16E-11	0.92	2602	1634	1.59

Theorem 3.5 proves that design order entropy conservative fluxes may be constructed using a linear combination of two-point entropy fluxes. A critical assumption used in the proof is that the two-point nondissipative fluxes satisfy Tadmor's integral relation given in (3.14). Herein, the nondissipative Euler fluxes of Ismail and Roe [24] are used. The study provides evidence that the nondissipative Euler fluxes of Ismail and Roe [24] do not degrade the formal accuracy. The interfaces are treated by using the entropy stable characteristic fluxes with a weighting parameter tuned to produce "upwind fluxes" at the interfaces. Design order convergence is achieved in all cases.

7.3.3. The viscous shock. The convergence rate for the viscous shock is evaluated on a properly nested sequence of uniform and nonuniform grids. The shock profile is initially located in the middle of the domain and is simulated until $t = 1.00$. The Reynolds number is $Re = 10$, and the reference Mach number is $M = 2.5$. The errors for the uniform and the nonuniform grids are shown in Table 3.

TABLE 3
Error convergence is shown for the one-dimensional Navier–Stokes equation.

	Uniform grid				Nonuniform grid			
$p = 01$	L^2 error	L^2 rate	L^∞ error	L^∞ rate	L^2 error	L^2 rate	L^∞ error	L^∞ rate
4	1.95E-01		5.92E-01		4.14E-01		1.19E-00	
8	7.11E-02	-1.46	2.73E-01	-1.11	1.81E-01	-1.19	7.30E-01	-0.71
16	2.10E-02	-1.76	9.51E-02	-1.53	5.26E-02	-1.78	2.52E-01	-1.53
32	5.57E-03	-1.92	2.57E-02	-1.89	1.51E-02	-1.80	8.85E-02	-1.51
64	1.42E-03	-1.97	6.50E-03	-1.98	4.05E-03	-1.91	2.40E-02	-1.88
128	3.58E-04	-1.99	1.63E-03	-1.99	1.03E-03	-1.97	6.06E-03	-1.98
$p = 02$								
4	2.64E-02		7.87E-02		1.02E-01		4.11E-01	
8	6.16E-03	-2.10	3.04E-02	-1.37	1.22E-02	-3.07	5.04E-02	-3.03
16	8.22E-04	-2.91	4.13E-03	-2.88	5.54E-03	-1.14	3.74E-02	-0.43
32	9.90E-05	-3.05	8.73E-04	-2.24	7.46E-04	-2.89	7.41E-03	-2.33
64	1.22E-05	-3.02	1.09E-04	-2.99	9.17E-05	-3.03	8.78E-04	-3.08
$p = 03$								
4	8.08E-03		4.73E-02		1.54E-02		3.60E-02	
8	4.94E-04	-4.03	3.93E-03	-3.59	7.22E-03	-1.09	5.53E-02	+0.62
16	3.45E-05	-3.84	3.77E-04	-3.38	3.86E-04	-4.22	4.03E-03	-3.78
32	2.12E-06	-4.03	2.47E-05	-3.93	2.89E-05	-3.74	4.00E-04	-3.34
64	1.28E-07	-4.05	1.46E-06	-4.08	1.76E-06	-4.04	2.58E-05	-3.95
$p = 04$								
4	1.33E-03		7.03E-03		1.16E-02		8.84E-02	
8	8.24E-05	-4.02	8.16E-04	-3.11	1.12E-03	-3.37	7.55E-03	-3.55
16	2.35E-06	-5.13	3.21E-05	-4.67	7.72E-05	-3.86	8.05E-04	-3.23
32	7.15E-08	-5.04	1.09E-06	-4.88	2.23E-06	-5.11	3.13E-05	-4.69
64	2.21E-09	-5.02	3.43E-08	-4.99	6.92E-08	-5.01	1.10E-06	-4.83

The interfaces are treated by using the entropy stable characteristic fluxes with a weighting parameter tuned to produce "upwind fluxes" at the interfaces. Design order convergence is achieved in both the L^2- and L^∞-norms on uniform and nonuniform grids.

The final smooth study simulates the two-dimensional viscous shock test problem on a properly nested sequence of nonuniform grids. The accuracy and efficiency of the *corrected* SSSCE scheme is compared with the baseline strong form nodal DG spectral operators. Design order accuracy is achieved in this study for both approaches; the nodal DG operators are slightly more accurate. The computational overhead of the correction approach increases with polynomial order from about 15% at $P = 1$ to about 40% at $P = 4$. Constructing the entropy fluxes accounts for a

large portion of the computational overhead (e.g., the SSSCE scheme alone suffers a 30% overhead relative to nodal DG, with the correction accounting for the remaining overhead). Note that relative overhead of the entropy stable formulation is smaller for the Navier–Stokes equations (i.e., compare Tables 2 and 4); the Stokes terms are a significant computational burden that partially amortizes the additional cost of corrected SSSCE scheme.

TABLE 4
Error convergence is shown for the two-dimensional Navier–Stokes equation.

	Nodal DG					SSSCE + correction					
$p = 01$	L^2 error	Rate	L^∞ error	Rate	Cost	L^2 error	Rate	L^∞ error	Rate	Cost	Overhead
008x008	9.95E-3		6.20E-2		-	1.02E-2		6.22E-2		-	-
016x016	5.17E-3	-0.94	5.97E-2	-0.05	-	5.35E-3	-0.93	5.32E-2	-0.22	-	-
032x032	2.04E-3	-1.34	2.58E-2	-1.20	-	2.23E-3	-1.26	2.70E-2	-0.97	-	-
064x064	6.08E-4	-1.74	7.69E-3	-1.74	19	7.13E-4	-1.64	8.07E-3	-1.74	20	1.05
128x128	1.54E-4	-1.98	2.08E-3	-1.88	200	1.79E-4	-1.99	2.20E-3	-1.87	210	1.05
256x256	3.87E-5	-1.99	5.19E-4	-2.00	2600	4.16E-5	-2.10	5.32E-4	-2.04	3088	1.18
$p = 02$											
008x008	1.79E-3		2.13E-2		-	1.84E-3		2.22E-2		-	-
016x016	4.20E-4	-2.08	7.35E-3	-1.53	-	4.45E-4	-2.04	7.85E-3	-1.49	-	-
032x032	7.40E-5	-2.50	1.09E-3	-2.75	7	7.82E-5	-2.50	1.27E-3	-2.62	9	0.99
064x064	8.70E-6	-3.08	1.55E-4	-2.81	138	9.22E-6	-3.08	1.69E-4	-2.90	168	1.21
128x128	1.14E-6	-2.92	2.27E-5	-2.76	1972	1.22E-6	-2.92	2.25E-5	-2.91	2346	1.18
$p = 03$											
008x008	2.48E-4		3.07E-3		-	2.73E-4		3.22E-3		-	-
016x016	2.32E-5	-3.42	5.96E-4	-2.36	-	2.59E-5	-3.39	6.11E-4	-2.39	-	-
032x032	1.53E-6	-3.92	6.12E-5	-3.28	45	1.71E-6	-3.92	6.25E-5	-3.28	47	1.04
064x064	9.22E-8	-4.05	2.42E-6	-4.66	557	1.02E-7	-4.06	2.76E-6	-4.49	764	1.37
$p = 04$											
008x008	3.41E-5		6.54E-4		-	3.71E-5		8.20E-4		-	-
016x016	1.51E-6	-4.49	4.81E-5	-3.76	5	1.70E-6	-4.44	5.73E-5	-3.83	8	1.41
032x032	5.03E-8	-4.90	1.47E-6	-5.03	102	5.70E-8	-4.89	1.79E-6	-5.00	147	1.43
064x064	1.67E-9	-4.91	6.69E-8	-4.45	2056	1.88E-9	-4.92	8.25E-8	-4.43	2876	1.39

7.4. Discontinuous tests. The following nomenclature is used to identify different permutations of the entropy stable schemes. The baseline uncorrected scheme of polynomial order three is denoted $SSSCE_{P3}$. An entropy correction based on the conventional DG scheme is denoted $SSSCE_{P3}$-DG.

7.4.1. Sod's test problem. The solution for Sod's problem is plotted at $t = 0.2$ in Figure 2. A numerical reference solution is obtained using 1024 uniformly distributed elements with the $SSSCE_{P3}$-DG scheme. For clarity, only two different algorithms are compared with the reference solution in each subfigure 2(a) and 2(b).

Figure 2(a) compares a conventional fourth-order energy stable weighted essentially nonoscillatory (ESWENO4) scheme [44] with the entropy corrected SSSCE scheme: $SSSCE_{P3}$-DG. A uniform distribution of 128 elements is used for the $SSSCE_{P3}$ scheme, while the ESWENO4 scheme uses a uniform distribution of points. Both simulations contain 512 degrees of freedom, and both algorithms are fourth-order accurate for smooth solutions.

Resolution of the expansion and contact discontinuity is adequate with either approach, with the $SSCE_{P3}$-DG scheme being less dissipative than the ESWENO4. The $SSSCE_{P3}$-DG scheme exhibits oscillations at the shock, although it captures the location correctly. Note that the only mechanisms for dissipation in the $SSSCE_{P3}$-DG scheme are (1) boundary conditions, (2) element interface upwinding, and (3) pointwise entropy correction of the fluxes; this is a remarkably low level of dissipation.

Figure 2(b) provides insight into the efficacy of the pointwise entropy correction of the fluxes. Compared is an *uncorrected* $SSSCE_{P3}$ scheme with the exact solution. Note the significant oscillations in the vicinity of the contact and the shock as compared with the $SSSCE_{P3}$-DG case shown in Figure 2(a). Also included in Figure 2(b) is the solution from an $SSSCE_{P9}$-DG scheme, run on an extremely coarse grid. Remarkably, even this combination provides reasonable resolution of the expansion

and contact waves. Again, oscillations are observed at the shock.

Neither the corrected nor the uncorrected SSSCE scheme experienced instability on this test problem for elements of polynomial order $1 \leq p \leq 9$. The entropy corrected algorithm always outperformed the uncorrected one in terms of smoothness of solution. The best results for the corrected algorithm were obtained in the range $3 \leq p \leq 4$. Note that the relative dissipation (dissipation per degree of freedom) introduced by flux upwinding at the element interfaces decreases with increased polynomial order. Inevitably, some form of hyperviscosity is required for extremely high polynomial orders; the baseline SSSCE scheme is entropy conservative and cannot be used to independently capture shocks.

Not shown are results obtained using the $SSSCE_{P3;5}$-MUSCL and $SSSCE_{P3}$-WENO schemes. Even the highly accurate $SSSCE_{P5}$-MUSCL corrected combination produced excessive smearing at the contact and shock, although oscillations at the shock were suppressed. The $SSSCE_{P3}$-WENO element correction was unsatisfactory on this test problem, indicating that stencil biasing into the adjoining elements is at the very least required.

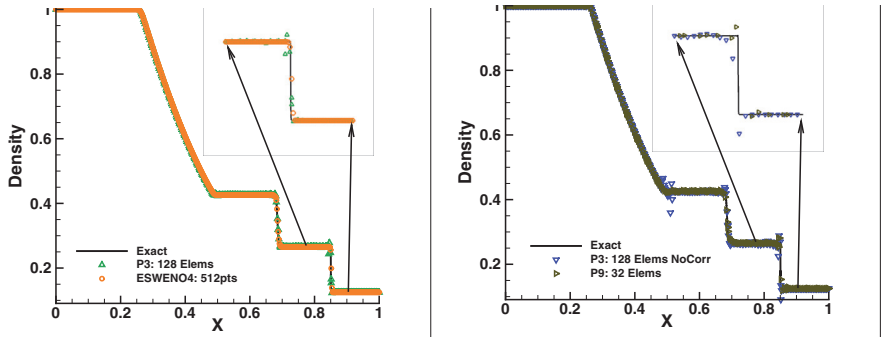

(a) Sod, $t = 0.2$ (b) Sod, $t = 0.2$

FIG. 2. *Density profiles for Sod's shock tube problem. Left subfigure compares ESWENO with the $SSSCE_{P3}$-DG scheme. Right subfigure compares the uncorrected $SSSCE_{P3}$ scheme with the $SSSCE_{P9}$-DG coarse grid scheme.*

7.4.2. Sine-shock test problem. The solutions for the interaction of a shock and a sinusoidal entropy wave are plotted at $t = 1.8$ in Figure 3. This test case exhibits a complex array of smooth and discontinuous features and provides insight into the potential of high-order shock capturing formulations. A numerical reference solution is obtained using 1024 uniformly distributed elements with the $SSSCE_{P3}$-DG scheme. Figure 3(a) compares the $SSSCE_{P3}$-DG scheme and the ESWENO4 scheme with an accurate reference solution, while Figure 3(b) compares the uncorrected $SSSCE_{P3}$ scheme and the coarse grid $SSSCE_{P9}$-DG scheme.

The algorithmic observations made in Sod's problem are equally valid for the sine-shock interaction problem. Figure 3(a) demonstrates the efficacy of the $SSSCE_{P3}$-DG scheme relative to the ESWENO4 scheme. The $SSSCE_{P3}$ scheme is less dissipative than the ESWENO4 scheme but experiences minor oscillations at the shock not present in the ESWENO4 solution. Figure 3(b) demonstrates the inadequacy of the uncorrected $SSSCE_{P3}$ scheme. Significant oscillations are present in the vicinity of the shocks. Similarly, the coarse grid $SSSCE_{P9}$-DG simulation shows inadequate resolution as well as oscillations in the vicinity of the shock. None of the simulations

exhibited numerical instability triggered by negative pressures.

The $SSSCE_{P5}$-MUSCL corrected combination produced excessive smearing of the smooth high frequency sinusoidal part of the solution. The work continues to develop a more discriminating shock sensor for this combination of operators.

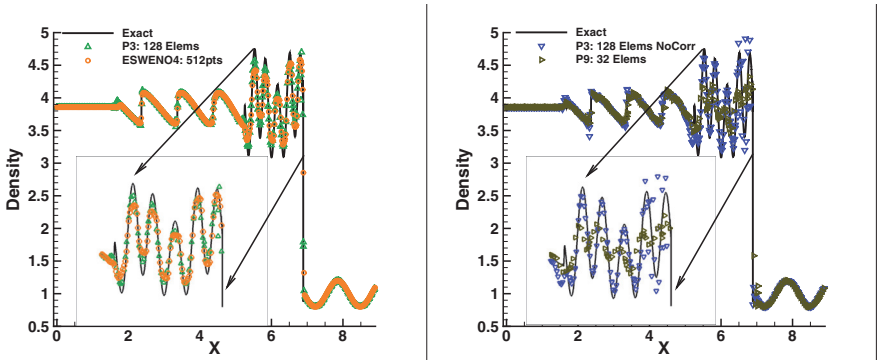

(a) Sine-shock interaction, $t = 1.8$. (b) Sine-shock interaction, $t = 1.8$.

FIG. 3. *Density profiles for the interaction of a shock and a sinusoidal entropy wave. Left subfigure compares ESWENO with the $SSSCE_{P3}$-DG scheme. Right subfigure compares the uncorrected $SSSCE_{P3}$ scheme with the $SSSCE_{P9}$-DG coarse grid scheme.*

7.4.3. Interacting blast waves. The collision of two shocks is used as the final discontinuous test problem. Recall that although the entropy stable discrete operators satisfy an L_2 entropy estimate (modulo boundary conditions), they still could experience pointwise instabilities triggered by negative pressures. This test problem is deliberately designed as a torture test with multiple discontinuous features, characterized by extremely large pressure discontinuities. An exact solution is not available for this case; a numerical reference solution is obtained using 1024 uniformly distributed elements with the $SSSCE_{P3}$-DG scheme.

The solutions for the interacting blast waves are plotted at $t = 0.038$ in Figure 4. This test case exhibits a complex array of smooth and discontinuous features. The blast waves test problem was successfully completed by $SSSCE_{Pp}$-DG schemes of polynomial orders $1 \leq p \leq 8$ on coarse grids. Only the $p <= 3$ formulations were stable on all grids. The failure mode typically occurred as the two waves met and negative pressures were encountered.

8. Conclusions. Entropy stable spectral collocation element (SSSCE) methods of arbitrary polynomial order are derived for the nonlinear Navier–Stokes equations. The discrete operators are formulated using a summation-by-parts (SBP) framework and are similar to strong form nodal DG spectral operators. The SSSCE schemes are strictly conservative for the Euler equations and also conserve the mathematical entropy over the element. Special entropy fluxes are used to achieve element entropy conservation. The individual entropy conservative spectral elements are coupled together in a conservative and entropy stable fashion using an SAT penalty approach. Characteristic upwinding is used for the inviscid fluxes; an entropy stable local discontinuous Galerkin (LDG) plus an internal penalty scheme are used to couple the viscous terms. A comparison approach is used to combine the SSSCE scheme with a conservative companion operator to produce an algorithm capable of capturing shocks.

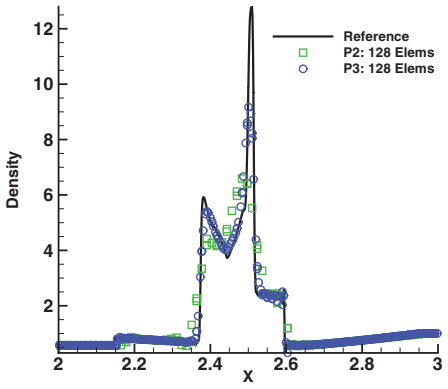

FIG. 4. *Density profiles for the interaction two blast waves. The figure compares two* $SSSCE_{P3}$*-DG schemes at different resolutions.*

The new operators are tested on both smooth and discontinuous test problems. All smooth test problems are shown to achieve design order accuracy of $p+1$ on the model problems. The discontinuous test problems are simulated with and without entropy corrections. It is shown that the base entropy conservative algorithm with upwinded interface fluxes is remarkably robust despite large oscillations at flow discontinuities. Entropy corrections derived from MUSCL, WENO, and conventional DG operators are tested. Remarkably little dissipation is needed to achieve satisfactory solutions for strong shocks.

REFERENCES

[1] D. N. ARNOLD, *An interior penalty finite element method with discontinuous elements*, SIAM J. Numer. Anal., 19 (1982), pp. 742–760.

[2] J. BERG AND J. NORDSTRÖM, *Stable Robin solid wall boundary conditions for the Navier-Stokes equations*, J. Comput. Phys., 230 (2011), pp. 7519–7532.

[3] M. H. CARPENTER AND T. C. FISHER, *Entropy Stable Spectral Collocation Schemes for the Navier-Stokes Equations: Discontinuous Interfaces*, Tech. report TM 218039, NASA, 2013.

[4] M. H. CARPENTER AND T. C. FISHER, *High-order entropy stable formulations for computational fluid dynamics*, in Proceedings of the 21st AIAA Computational Fluid Dynamics Conference, San Diego, CA, 2013, AIAA 2013-2868.

[5] M. H. CARPENTER AND D. GOTTLIEB, *Spectral methods on arbitrary grids*, J. Comput. Phys., 129 (1996), pp. 74–86.

[6] M. H. CARPENTER, D. GOTTLIEB, AND S. ABARBANEL, *Time-stable boundary conditions for finite-difference schemes solving hyperbolic systems: Methodology and application to high-order compact schemes*, J. Comput. Phys., 111 (1994), pp. 220–236.

[7] M. H. CARPENTER AND C. A. KENNEDY, *Fourth-Order* $2N$*-Storage Runge-Kutta Schemes*, Tech. report TM 109112, NASA, 1994.

[8] M. H. CARPENTER, J. NORDSTRÖM, AND D. GOTTLIEB, *A stable and conservative interface treatment of arbitrary spatial accuracy*, J. Comput. Phys., 148 (1999), pp. 341–365.

[9] M. H. CARPENTER, J. NORDSTRÖM, AND D. GOTTLIEB, *Revisiting and extending interface penalties for multi-domain summation-by-parts operators*, J. Sci. Comput., 45 (2009), pp. 118–150.

[10] B. COCKBURN AND C.-W. SHU, *The local discontinuous Galerkin method for time-dependent convection-diffusion systems*, SIAM J. Numer. Anal., 35 (1998), pp. 2440–2463.

[11] T. C. FISHER, *High-Order* L^2 *Stable Multi-Domain Finite Difference Method For Compressible Flows*, Ph.D. thesis, Purdue University, West Lafayette, IN, 2012.

[12] T. C. FISHER AND M. H. CARPENTER, *High-Order Entropy Stable Finite Difference Schemes for Nonlinear Conservation Laws: Finite Domains*, Tech. report TM 217971, NASA, 2013.

[13] T. C. Fisher and M. H. Carpenter, *High-order entropy stable finite difference schemes for nonlinear conservation laws: Finite domains*, J. Comput. Phys., 252 (2013), pp. 518–557.
[14] T. C. Fisher, M. H. Carpenter, J. Nordström, N. K. Yamaleev, and R. C. Swanson, *Discretely Conservative Finite-Difference Formulations for Nonlinear Conservation Laws in Split Form: Theory and Boundary Conditions*, Tech. report TM 2011-217307, NASA, 2011.
[15] T. C. Fisher, M. H. Carpenter, J. Nordström, N. K. Yamaleev, and R. C. Swanson, *Discretely conservative finite-difference formulations for nonlinear conservation laws in split form: Theory and boundary conditions*, J. Comput. Phys., 234 (2013), pp. 353–375.
[16] U. S. Fjordholm, S. Mishra, and E. Tadmor, *Arbitrarily high-order accurate entropy stable essentially nonoscillatory schemes for systems of conservation laws*, SIAM J. Numer. Anal., 50 (2012), pp. 544–573.
[17] G. J. Gassner, *A skew-symmetric discontinuous Galerkin spectral element discretization and its relation to SBP-SAT finite difference methods*, SIAM J. Sci. Comput., 35 (2013), pp. A1233–A1253.
[18] S. K. Godunov, *An interesting class of quasi-linear systems*, Dokl. Akad. Nauk SSSR, 139 (1961), pp. 521–523 (in Russian).
[19] A. Harten, *On the symmetric form of systems of conservation laws with entropy*, J. Comput. Phys., 49 (1983), pp. 151–164.
[20] A. Harten, B. Engquist, S. Osher, and S. R. Chakravarthy, *Uniformly high order accurate essentially non-oscillatory schemes,* III, J. Comput. Phys., 71 (1987), pp. 231–303.
[21] J. S. Hesthaven and T. Warburton, *Nodal Discontinuous Galerkin Methods: Algorithms, Analysis, and Applications*, Texts Appl. Math. 54, Springer, New York, 2008.
[22] J. S. Hesthaven and D. Gottlieb, *A stable penalty method for the compressible Navier–Stokes equations:* I. *Open boundary conditions*, SIAM J. Sci. Comput., 17 (1996), pp. 579–612.
[23] T. J. R. Hughes, L. P. Franca, and M. Mallet, *A new finite element formulation for computational fluid dynamics.* I. *Symmetric forms of the compressible Euler and Navier-Stokes equations and the second law of thermodynamics*, Comput. Methods Appl. Mech. Engrg., 54 (1986), pp. 223–234.
[24] F. Ismail and P. L. Roe, *Affordable, entropy-consistent Euler flux functions* II*: Entropy production at shocks*, J. Comput. Phys., 228 (2009), pp. 5410–5436.
[25] G. Jiang and C.-W. Shu, *Efficient implementation of weighted ENO schemes*, J. Comput. Phys., 126 (1996), pp. 202–228.
[26] D. A. Kopriva, *Implementing Spectral Methods for Partial Differential Equations*, Springer, New York, 2009.
[27] B. Koren, *A robust upwind discretisation method for advection, diffusion and source terms*, in Numerical Methods for Advection-Diffusion Problems, C. B. Vreugdenhil and B. Koren, eds., Vieweg, Braunschweig, Wiesbaden, 1993, pp. 117–138.
[28] P. D. Lax, *Hyperbolic Systems of Conservation Laws and the Mathematical Theory of Shock Waves*, SIAM, Philadelphia, 1973.
[29] P. G. LeFloch, *Hyperbolic Systems of Conservation Laws: The Theory of Classical and Nonclassical Shock Waves*, Birkhäuser Verlag, Basel, 2002.
[30] P. G. LeFloch, J. M. Mercier, and C. Rohde, *Fully discrete, entropy conservative schemes of arbitrary order*, SIAM J. Numer. Anal., 40 (2002), pp. 1968–1992.
[31] X.-D. Liu, S. Osher, and T. Chan, *Weighted essentially non-oscillatory schemes*, J. Comput. Phys., 115 (1994), pp. 200–212.
[32] M. L. Merriam, *An Entropy-Based Approach to Nonlinear Stability*, Tech. report TM 101086, NASA, 1989.
[33] M. S. Mock, *Systems of conservation laws of mixed type*, J. Differential Equations, 37 (1980), pp. 70–88.
[34] J.Nordström, J. Gong, E. van der Weide, and M. Svärd, *A stable and conservative high order multi-block method for the compressible Navier-Stokes equations*, J. Comput. Phys., 228 (2009), pp. 9020–9035.
[35] R. LeVeque, *Numerical Methods for Conservation Laws*, 2nd ed., Birkhäuser Verlag, Basel, 1992.
[36] C.-W. Shu and S. Osher, *Efficient implementation of essentially non-oscillatory shock-capturing schemes*, J. Comput. Phys., 77 (1988), pp. 439–471.
[37] M. Svärd, M. H. Carpenter, and J. Nordström, *A stable high-order finite difference scheme for the compressible Navier-Stokes equations, far-field boundary conditions*, J. Comput. Phys., 225 (2007), pp. 1020–1038.
[38] M. Svärd and J. Nordström, *On the order of accuracy for difference approximations of initial-boundary value problems*, J. Comput. Phys., 218 (2006), pp. 333–352.

[39] M. Svärd and Hatice Özcan, *Entropy-stable schemes for the Euler equations with far-field and wall boundary conditions*, J. Sci. Comput., 58 (2014), pp. 61–89.
[40] E. Tadmor, *The numerical viscosity of entropy stable schemes for systems of conservation laws.* I, Math. Comp., 49 (1987), pp. 91–103.
[41] E. Tadmor, *Entropy stability theory for difference approximations of nonlinear conservation laws and related time-dependent problems*, Acta Numer., 12 (2003), pp. 451–512.
[42] M. F. Wheeler, *An elliptic collocation-finite element method with interior penalties*, SIAM J. Numer. Anal., 15 (1978), pp. 152–161.
[43] P. Woodward and P. Colella, *The numerical simulation of two-dimensional fluid flow with strong shocks*, J. Comput. Phys., 54 (1984), pp. 115–173.
[44] N. K. Yamaleev and M. H. Carpenter, *Third-order energy stable WENO scheme*, J. Comput. Phys., 228 (2009), pp. 3025–3047.